PRODUCTION OF A HIGHLY-IONIZED GAS BY AN ELECTROMAGNETICALLY-DRIVEN SHOCK WAVE

by

GEORGE DOUGLAS CORMACK

B.A.Sc., University of British Columbia, 1955

A THESIS SUBMITTED IN PARTIAL FULFILMENT OF

THE REQUIREMENTS FOR THE DEGREE OF

M.Sc.

in the Department

of

PHYSICS

We accept this thesis as conforming to the

required standard

THE UNIVERSITY OF BRITISH COLUMBIA

October, 1960

In presenting this thesis in partial fulfilment of the requirements for an advanced degree at the University of British Columbia, I agree that the Library shall make it freely available for reference and study. I further agree that permission for extensive copying of this thesis for scholarly purposes may be granted by the Head of my Department or by his representatives. It is understood that copying or publication of this thesis for financial gain shall not be allowed without my written permission.

Department of Physics

The University of British Columbia,
Vancouver 8, Canada.

Date October 1, 1960

ABSTRACT

A study has been made of the properties of an electromagnetically generated shock wave travelling through both argon and helium. An initial capacitive energy of 450 joules has been rapidly discharged into the gas and has resulted in shock wave velocities of up to five centimeters per microsecond. The high velocities obtained can be attributed to careful design of the main discharge circuit.

Preliminary results of measurements of the properties of the shock wave are given. Of primary interest has been the results of measurements of the properties of the plasma associated with the shock wave. A magnetic field deflection method has been developed for the measurement of the electrical conductivity of this plasma.

TABLE OF CONTENTS

ILLUSTRATIONS

TABLES

ACKNOWLEDGEMENTS

The author wishes to express his gratitude to Dr. A.J. Barnard for his generous assistance and guidance.

A warm thank you is also given to Dr. K. Sodomsky for many helpful discussions and to Dr. G.V. Bull, Canadian Armament Research and Development Establishment, who has been responsible for introducing the author to this extremely interesting and important field of Plasma Physics.

I INTRODUCTION

The possibility of harnessing the energy released by a fusion reaction is one of the most tantalizing aims of present-day scientific research. Scientists in this field of study have realized that they are tackling a far more difficult problem than that posed by the harnessing of a fission reaction. Their attention is now centered not primarily on the fusion reaction itself, but rather on the conditions for obtaining an efficient reaction rate. Because the most promising reaction will only proceed efficiently at temperatures in excess of 10^8 °K. according to Bishop (1958), the constituents must be highly ionized and of course in gaseous form. Such highly ionized gases are called plasmas and the study of their properties, plasma physics.

There is much to be known of the properties of plasmas. In his efforts to harness this energy source of the stars, man has had to compromise and study not the hot, long-lived plasmas that he would wish to study, but rather the attainable alternatives of either a cool, long-lived plasma or a hot, short-lived plasma. In either case he is hampered by his lack of complete knowledge of the properties of a plasma.

One method of generating a plasma under conditions that are fairly amenable to analysis is to ionize a gas with a shock wave. It is this method that has been developed in the work upon which this thesis is based. Gas atoms are abruptly heated by the shock front and then slowly impart their heat energy into excitation and ionization energy until temperature

equilibrium between the constituents of the gas is attained. Subsequent cooling then decreases the temperature of all constituents and the degree of ionization. The time interval during which the gas is ionized is of the order of one to ten microseconds, quite sufficient for spectrographic, photometric and electronic observations to be made. Design considerations are given in this thesis for both the high energy electrical discharge shock driving equipment and the equipment used for measuring the properties of the shock wave, including the plasma following the shock front. Preliminary results of measurements obtained with this equipment are also presented.

In a conventional shock tube a low pressure section is separated from a high pressure section by a thin diaphragm. The diaphragm is ruptured by slowly increasing the pressure differential until the diaphragm breaks. The shock wave thus generated then travels down the low pressure section of the shock tube. The characteristics of a conventional shock tube are reviewed by Penner, Harshburger and Vali (1957).

A conventional shock tube was used by Resler, Lin and Kantrowitz (1952) to study the properties of argon at thermal equilibrium temperatures of up to 18,000°K. Their studies reached fruition with the publication of the papers by Petschek, Rose et al (1955) and Lin, Resler and Kantrowitz (1955). They were interested in spectral line broadening and line shifts, continuum radiation and the conductivity of the plasma associated with the shock wave. The method that they employed to measure the electrical conductivity has been adopted in the present work. The method consists of allowing the shock wave to pass through a radial magnetic field. The force on the electrons results in a circumferential current which can be

- to follow page 2 -

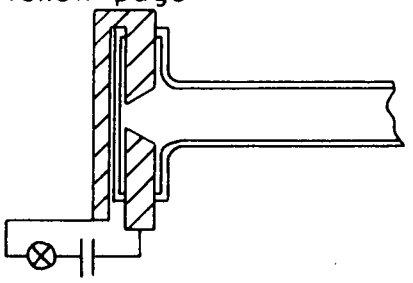

1a : T - Tube Driver

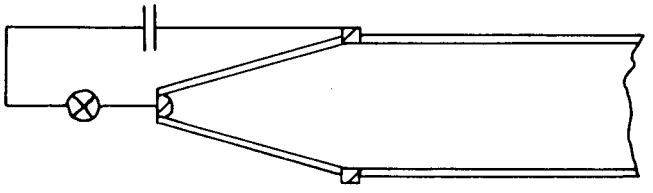

1b : Conical Driver

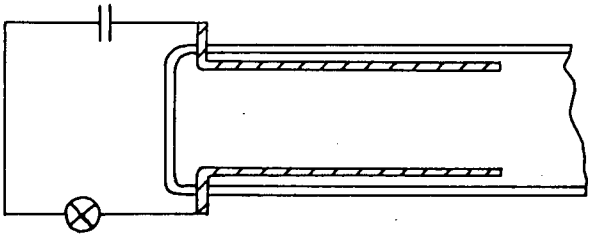

1c : Rail Driver

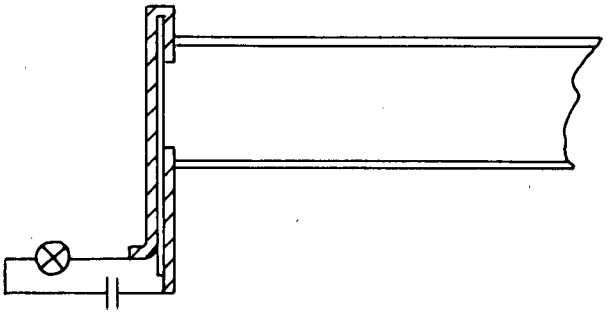

1d : Co-planar Driver

Figure 1 : Electromagnetic Drivers

measured by transformer action into a pick-up coil. The output voltage from the coil can then be related to the conductivity of the plasma. Petschek (1957) presented both experimental data and a theoretical analysis on the ionization processes that occur in argon after the passage of a strong shock wave which has been generated in a conventional shock tube.

The temperature that can be obtained in a conventional shock tube is limited by the thermodynamic properties of the driving gases. A higher temperature can be obtained by adding an explosive to the high pressure section. The maximum temperature will again be limited by such factors as the burning rate of the explosive and the thermodynamic properties of each of the gases in the system.

The highest temperature behind a shock wave can be obtained by generating the shock wave by electromagnetic means. Fowler et al (1952) first proposed that strong shock waves could be generated by an electrical discharge. This method consists of very quickly depositing the energy of a charged condenser bank into the gas that is between two electrodes at one end of a shock tube. The electrical discharge that occurs between the electrodes generates a shock wave. Kolb (1957) introduced the T-Tube driver (Figure 1a) that utilizes the Lorentz force caused by close coupling between the current-return conductor and the discharge in the gas to give additional driving energy to the shock front. Kolb studied the properties of very high energy shock waves passing through deuterium. He was unable, however, to measure the temperature of the high temperature gas associated with the shock wave. In a subsequent publication Kolb (August 1957) discusses a successful method of increasing the velocity of the shock wave by applying a strong longitudinal magnetic field to the shock wave while it is leaving the

main discharge chamber. Kolb (1958) has also experimented with colliding shock waves and has by this means obtained temperatures of about 2×10^6 °K., as deduced from the shock velocities. Josephson (1958) studied the properties of the conical driver shown in Figure 1(b). The advantage of this system over that of Kolb was that this driver was symmetrical thus more likely ensuring in the formation of a plane shock front. A plane shock front will travel down a shock tube with less attenuation than a non-plane shock front, because the radially-travelling energy in a non-plane shock front will be attenuated upon reflection from the walls. Josephson also studied the shock driving properties of an electrodeless discharge which he obtained by discharging the energy of a charged condenser bank into a coil wrapped around one end of the shock tube. The intense field in the gas caused by the coil resulted in breakdown of the gas, absorption of energy and then the generation of a shock wave that had the characteristic of being free of electrode contamination. Hart (1960) experimentally optimized the angle of the cone that was used in a driving assembly quite similar to that of Josephson and also experimented with various cone materials. The rail drive method (Figure 1(c)) is discussed by Bostick (1958). The driver that has been developed for the present work is shown in Figure 1 (d). This driver is similar to that used by Kolb (1957) but is more efficient because a closer coupling has been employed between the current-return conductor and the discharge in the gas.

All experiments have been of an exploratory nature in order that familiarily with techniques may be gained and a firm foundation laid for more elaborate experiments. The work to date has been somewhat hampered by lack of equipment. In particular, the condenser bank that has been employed is

quite slow and has a very low energy storage capacity - 450 joules. Nevertheless, very careful design of the main discharge circuit has resulted in the achievement of comparable temperatures, as deduced from the velocity of the shock front, to those obtained by Kash et al (1958) who employed a far faster condenser bank. The experimental measurements on the shock wave have been concerned with obtaining time-integrated emission spectra transverse to the shock tube, distance-time relations for the luminosity associated with the shock wave and conductivity-position relations for the plasma associated with the shock wave.

The investigation has been concerned with shock waves in argon and helium possessing sufficient energy to heat the unexcited, un-ionized gas atoms immediately behind the shock front to a maximum temperature of about 400,000°K. One of the objects of the investigation has been to make a detailed study of the properties of shock waves in argon which produce a higher temperature than that considered (27,000°K. immediately behind the shock front) by Petschek, Rose et al (1955) and Petschek (1957).

The present apparatus can be readily modified to yield far higher temperatures by replacement of the present condenser bank with a bank possessing less inductance and higher energy storage capacity. These superior condensers will be installed as soon as they become available.

– to follow page 5 –

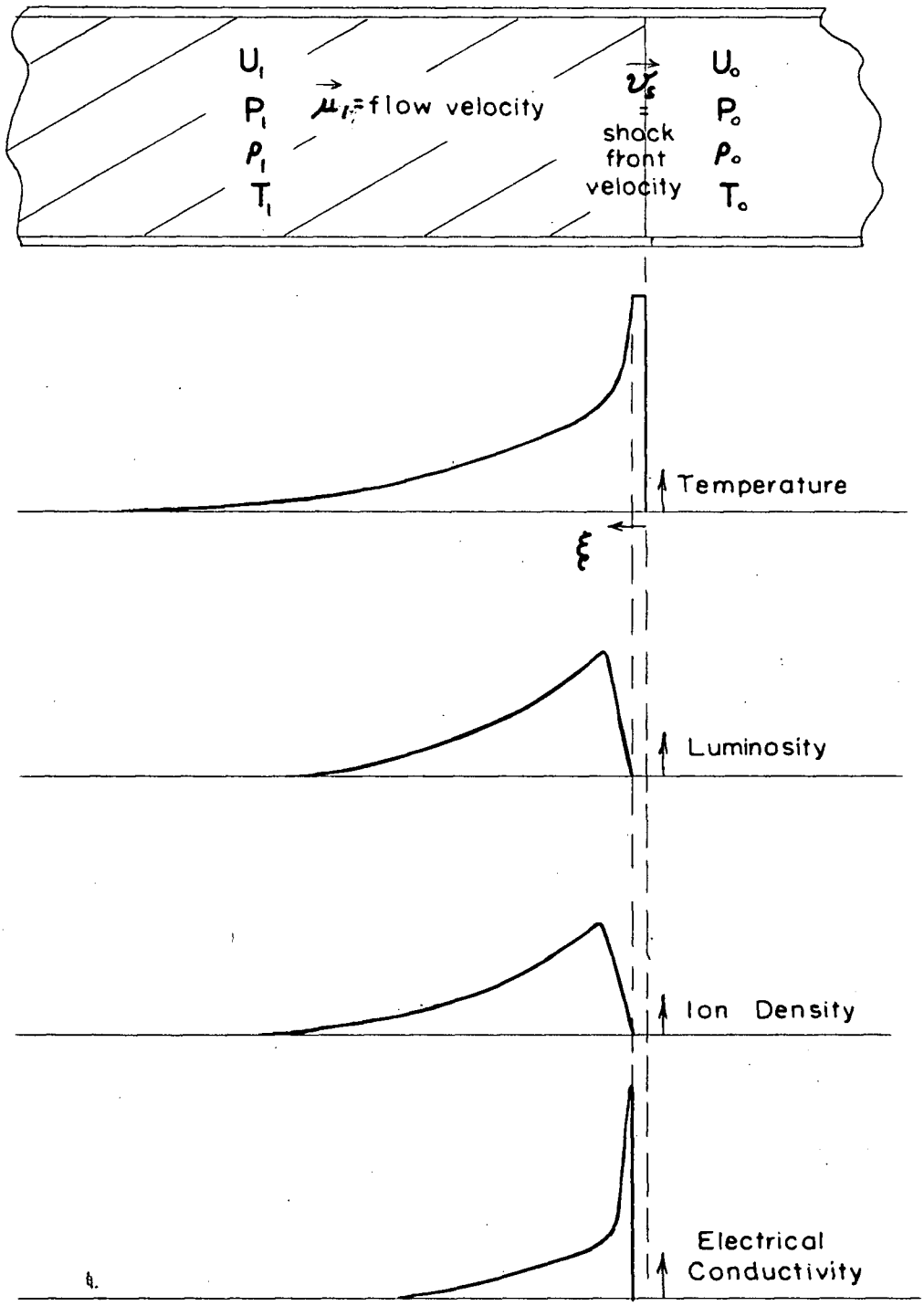

Figure 2: Characteristics of a Strong Shock Wave

$$\mathcal{M}\, U = C_v T \tag{5}$$

or

$$U = \frac{1}{\gamma - 1} R_1 T \tag{6}$$

where $\mathcal{M}$ = molecular weight of gas and $R_1 \mathcal{M} = C_p - C_v = R$ = gas constant per mole = 8.315×10^7 ergs per $^\circ$K. mole (Perry, 1941), when P is expressed in dynes/sq. cm. and ρ in grams/cm.^{3}. For an ideal monatomic gas $\gamma = 5/3$. For argon there is considerable departure from this value at high pressures. Representative of the values quoted by Din (1956) are, $\gamma = 1.640$ for P = 1 atmosphere and T = 90°F., $\gamma = 1.669$ for P = 1 atmosphere and T = 600°F., $\gamma = 1.793$ for P = 200 atmospheres and T = 600°F. The value of $\gamma = 5/3$ for both argon and helium (Perry, 1941) over the pressure temperature range of interest appears to be quite justified.

Equations 1 to 6 can be solved for T_1, P_1, ρ_1, and u_1 in terms of the velocity of the shock front and the variables P_0 and ρ_0. For strong shock waves $P_1 \gg P_0$ and $U_1 \gg U_0$ and the equations reduce to

$$T_1 = \frac{2(\gamma - 1)}{(\gamma + 1)^2} \frac{v_s^2}{R_1} \tag{7}$$

$$u_1 = \frac{3}{4} v_s \tag{8}$$

$$P_1 = \frac{2 \rho_0}{\gamma + 1} v_s^2 \tag{9}$$

$$\rho_1 = \frac{\gamma + 1}{\gamma - 1} \rho_0 \tag{10}$$

Or, when $\gamma = 5/3$:

$$T_1 = \frac{3}{16} \frac{v_s^2}{R_1} \tag{11}$$

$$u_1 = \frac{3}{4} v_s \tag{12}$$

$$P_1 = \frac{3}{4} \rho_0 v_s^2 \tag{13}$$

$$\rho_1 = 4 \rho_0 \tag{14}$$

Alternatively these equations may be expressed as functions of Mach number in the undisturbed gas at temperature T_0,

$$M = \frac{v_s}{v_{sound}} = \frac{v_s}{\sqrt{\gamma R_1 T_0}} \tag{15}$$

where $R_1 = \frac{8.315 \times 10^7}{39.944}$ ergs/°K.gm. for v_{sound} to be measured in cms./sec. in argon.

2. <u>Low Degree of Ionization</u>

Resler, Lin and Kantrowitz (1952) consider this case and state that the internal energy of the gas when radiation is neglected is given by,

$$U = \frac{1}{\gamma - 1} R_1 T (1 + \alpha) + \alpha \times \frac{R_1}{k} \tag{16}$$

Here α is the fraction of the original monatomic gas which is singly ionized at a given temperature and pressure, k is Boltzmann's constant 8.616×10^{-5} ev./°K. and x is the ionization energy in electron volts. The first term on the right hand side of this equation represents the internal energy of the atom, ion and electron gas, there being $1 + \alpha$ times as many particles in the ionized gas having three degrees of freedom as in the un-ionized gas. The second term represents the internal energy that is due to ionization. Excitation and dissociation contributions to the internal energy are neglected in this equation. For a monatomic gas such as argon or helium, there is of course no dissociation energy.

The variable α introduced in equation 16 must be determined from an additional equation of state. One approach to this problem is to assume

that thermodynamic equilibrium holds for the ionization and recombination reactions that determine the density of ions and electrons in the gas. Saha's equation then yields the relation (Lin, Resler and Kantrowitz, 1955),

$$\alpha = G \frac{T^{5/4}}{p^{1/2}} e^{\frac{-x}{2kT}} \tag{17}$$

where G is a constant which for argon equals 1.73×10^{-2} when T is in °K. and p in centimeters of mercury. Guman (1958) considers in more detail the equations for a shock wave than do Lin, Resler and Kantrowitz (1955), but unfortunately also assumes that Saha's equation is valid. There is considerable doubt that Saha's equation is valid for the conditions in the high temperature gas following a shock wave because the gas is not in an isolated system. The gas is continually losing photons and the reactions that are believed to proceed do not proceed to equilibrium concentrations of the constituents,

$$X + h\nu \rightleftarrows X^+ + e \tag{18}$$

$$X + e \rightleftarrows X^+ + 2e \tag{19}$$

where x represents an atom of the gas considered.

3. High Degree of Ionization

When the gas behind the shock front is highly ionized, the shock wave will have the characteristics shown in Figure 2.

It is very little trouble to extend the analysis of Petschek and Byron (1957) to be applicable for the description of a shock wave which is sufficiently strong to result in multiple-ionization and any degree of ionization. Excitation energy could be included as an extra term of the form $\sum \beta_i y_i \frac{R_1}{k}$ in the internal energy equation. However, since excitation

energies would be quite difficult to measure in the present apparatus, the present analysis will neglect excitation energy. $\beta_i y_i$ would be the excitation energy per gram of the gas atoms which have the excitation energy y_i and β_i would be the fraction of the original gas atoms that have the excitation energy y_i. Let α_i = fraction of the initial gas which is i^{th}-ionized, X_i = ionization potential of the ith-ionized ion. Then for $P_1 \gg P_0$, $U_1 \gg U_0$,

$$\rho_0 v_s = \rho_1 (v_s - u_1) = m \tag{20}$$

$$P_1 = m u_1 \tag{21}$$

$$m\left(U_1 + \frac{1}{2} u_1^2\right) = P_1 u_1 \tag{22}$$

$$P_1 = \left(1 + \Sigma i \alpha_i\right) \rho_1 R_1 T_1 \tag{23}$$

$$U_1 = \frac{1}{\gamma - 1} R_1 T_1 \left(1 + \Sigma i \alpha_i\right) + \Sigma \alpha_i X_i \frac{R_1}{k} \tag{24}$$

From equations 21 and 22,

$$U_1 = \frac{1}{2} u_1^2 \tag{25}$$

The temperature T behind the shock front is desired as a function of v_s and α_i, so a solution of the above five equations for u_1 and T_1 yields,

From equations 20 and 21,

$$P_1 = \rho_1 (v_s - u_1) u_1 \tag{26}$$

From equations 23 and 26,

$$\left(1 + \Sigma i \alpha_i\right) R_1 T_1 = (v_s - u_1) u_1 \tag{27}$$

From equations 24 and 25,

$$\frac{1}{2} u_1^2 = \frac{1}{\gamma - 1} R_1 T_1 \left(1 + \Sigma i \alpha_i\right) + \Sigma \alpha_i X_i \frac{R_1}{k} \tag{28}$$

u_1 as a function of v_s and α_i is found by combining equations 27 and 28,

$$u_1^2 = \frac{2}{\gamma-1} u_1 (v_s - u_1) + 2 \sum \alpha_i x_i \frac{R_1}{k} \tag{29}$$

In particular, if $\gamma = 5/3$,

$$u_1^2 = 3 u_1 v_s - 3 u_1^2 + 2 \sum \alpha_i x_i \frac{R_1}{k} \tag{30}$$

Therefore,

$$4 u_1^2 - 3 u_1 v_s - 2 \sum_i \alpha_i x_i \frac{R_1}{k} = 0$$

or

$$u_1 = \frac{3 v_s + \sqrt{9 v_s^2 - 32 \sum \alpha_i x_i \frac{R_1}{k}}}{8} \tag{31}$$

Combining equations 27 and 31 yields the desired equation for T_1,

$$T_1 = \frac{1}{64 R_1 (1 + \sum i \alpha_i)} \left(5 v_s - \sqrt{9 v_s^2 - 32 \sum \alpha_i x_i \frac{R_1}{k}}\right)\left(3 v_s + \sqrt{9 v_s^2 - 32 \sum \alpha_i x_i \frac{R_1}{k}}\right) \tag{32}$$

It is of interest to calculate the value of u_1 from equation 31 for singly-ionized argon (x_1 = 15.75 ev.),

$$u_1 = \frac{3 v_s + \sqrt{9 v_s^2 - 12.18 \times 10^{12} \alpha_1}}{8} \tag{33}$$

For helium (x_1 = 24.58 ev.),

$$u_1 = \frac{3 v_s + \sqrt{9 v_s^2 - 189.3 \times 10^{12} \alpha_1}}{8} \tag{34}$$

Once more an additional relation between α_1 and T is needed. Petschek and Byron (1957) have obtained a relation by balancing the rate of change of the thermal energy of the electrons with the net rate of energy input to the electron gas. The net rate of energy input to the electron gas

is controlled by elastic collisions between the electrons and the atoms and ions in the gas. The rate of energy loss by the electrons is controlled by electron-atom collisions. Knorr (1958) has derived a general expression that is applicable for multiple-ionization and that relates α_i to T by considering equilibrium between the photo-recombination and ionization by collision reactions included in equations 18 and 19. It is beyond the scope of this thesis to consider these theories in detail or to either expand or adapt them to be applicable to the high temperature conditions obtained in the present apparatus.

One point that should now be mentioned is that at the high temperatures now obtained, there will be appreciable radiation loss. An adequate theory yielding a relation between T and α (or T and α_i for multiple-ionization) should include consideration of the loss of de-excitation and de-ionization photons and continuum radiation.

Figure 3 : Shock Tube

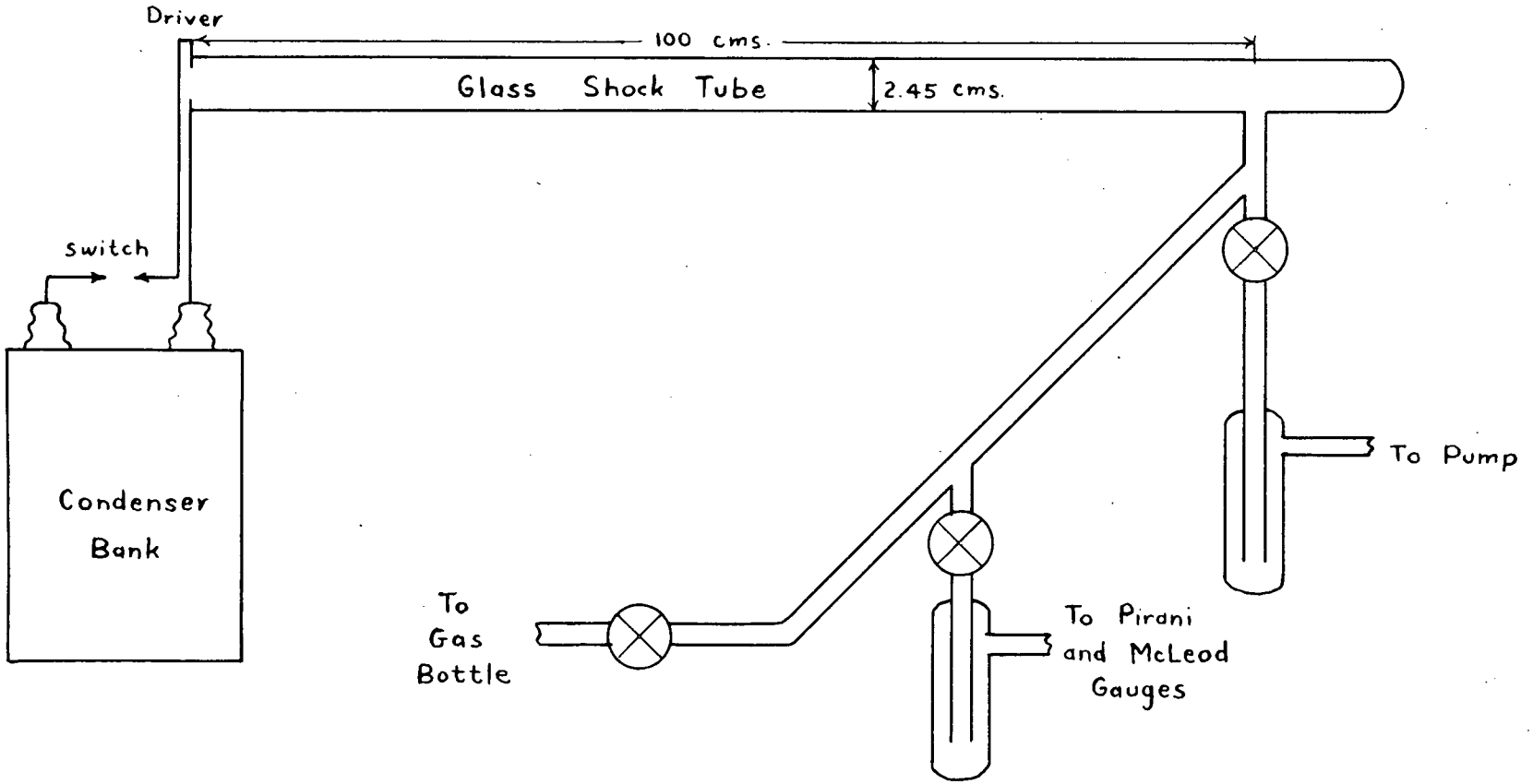

- to follow page 12 -

III APPARATUS

1. General

A schematic showing the dimensions and layout of the shock tube is given in Figure 3. Not shown is a grounded shield enclosing the main discharge circuit and consisting of a box made of 1/32 inch thick aluminum sheeting.

The shock tube was evacuated with a Cenco Hi Vac 14 mechanical pump rated at 0.1 microns. The lowest system pressure that could actually be obtained was 0.1 microns. The working evacuation pressure before admission of argon (99.98% pure) or helium (unknown purity) was about 1 micron. The minimum system pressure during firing was 500 microns and the pressure rise due to firing was then about 90 microns. The concentration of impurities in the ambient argon gas in front of the shock wave was, therefore, equal to or less than 6×10^{-4}. Pressures were read from a Pirani Gauge which was periodically standardized against a McLeod Gauge. The spectrum of the luminosity emitted by the shock wave contained no lines that could be attributed to gaseous impurities. A more elaborate pumping system was, therefore, not justified.

The high voltage power supply was a N.J.E. Corporation 0-30 KV. Model H-51 unit.

Electrical signals were observed with two Tektronix oscilloscopes, one type 535 and one type 551. The pre-amplifiers that have been used in

– to follow page 13 –

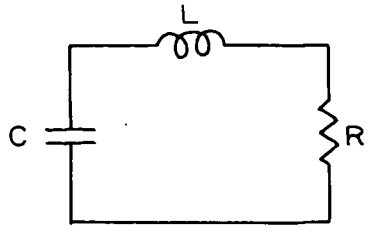

4a : Single Components

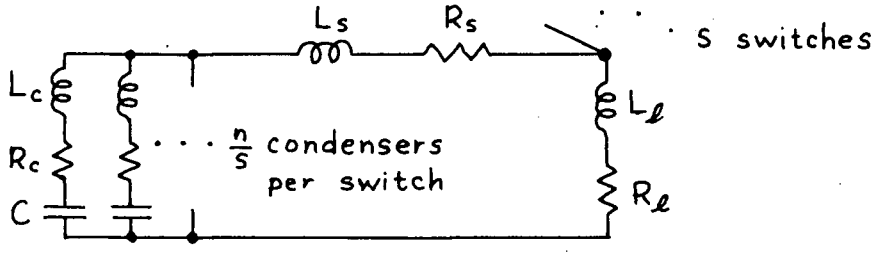

4b : Multiple Components

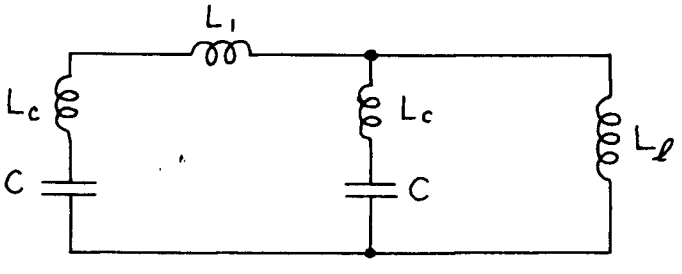

4c : Shared Inductance

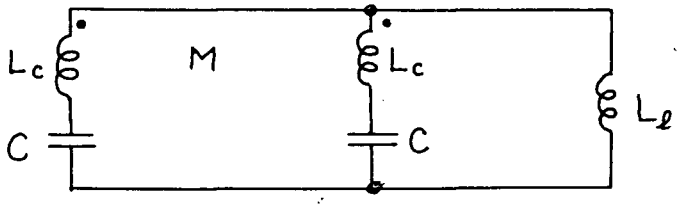

4d : Mutual Inductance

Figure 4 : Discharge Circuits

these oscilloscopes have included types G, K and 53/54 D. Permanent records of signals have been obtained with a Dumont polaroid oscilloscope camera.

2. Main Discharge Circuit

The shock wave is driven by an electrical discharge. The parameters of importance in the discharge circuit are the rise-time of the current, the energy stored and the ratio of load to lead resistance. A preliminary observation of the current waveform revealed that it was essentially a damped sinusoid. The simplest equivalent circuit that will result in this current waveform is a circuit having non-time-dependent components and consisting of a series resistance, capacitance and inductance. The following analysis applies to such a circuit (See Figure 4a),

$$LC \frac{d^2 i}{dt^2} + 2\delta LC \frac{di}{dt} + i = 0 \tag{35}$$

$$i\,(t=0) = 0 \tag{36}$$

$$\frac{di}{dt}\,(t=0) = \frac{V_o}{L} \tag{37}$$

The general solution for equations 35 to 37 for an underdamped discharge is,

$$i(t) = \frac{V_o}{\omega L}\, e^{-\delta t} \sin \omega t \tag{38}$$

where ω = cyclic frequency $= \sqrt{\frac{1}{LC} - \delta^2}$ and δ = damping coefficient = $\frac{R}{2L}$.

The power dissipated in the resistance has the form,

$$P(t) = \left(\frac{V_o}{\omega L}\right)^2 R\, e^{-2\delta t} \sin^2 \omega t \tag{39}$$

Both the power and the current have maxima when $\frac{di}{dt} = 0$ or when,

$$\tan \omega t = \frac{\omega}{\delta} \tag{40}$$

The extension of this analysis to the case of multiple condensers and spark gaps (Figure 4b) is readily made and yields the results,

$$i_\ell(t) = \frac{V_o}{\omega\left(\frac{L_s}{s} + \frac{L_c}{n} + L_\ell\right)} e^{-\delta t} \sin \omega t \tag{41}$$

$$P_\ell(t) = \left[\frac{V_o}{\omega\left(\frac{L_s}{s} + \frac{L_c}{n} + L_\ell\right)}\right]^2 R_\ell \, e^{-2\delta t} \sin^2 \omega t \tag{42}$$

where

$$\delta = \frac{\frac{R_s}{s} + \frac{R_c}{n} + R_\ell}{2\left(\frac{L_s}{s} + \frac{L_c}{n} + L_\ell\right)} \tag{43}$$

and

$$\omega = \sqrt{\frac{1}{nC\left(\frac{L_s}{s} + \frac{L_c}{n} + L_\ell\right)} - \delta^2} \tag{44}$$

Note that the damped period of the waveform is,

$$\tau = \frac{2\pi}{\sqrt{\frac{1}{nC\left(\frac{L_s}{s} + \frac{L_c}{n} + L_\ell\right)} - \delta^2}} \tag{45}$$

and the undamped period,

$$\tau = 2\pi\sqrt{nC\left(\frac{L_s}{s} + \frac{L_c}{n} + L_\ell\right)} \tag{46}$$

The maximum current and maximum power dissipated in the load occur when $\frac{di}{dt} = 0$ or when $\tan wt = \frac{\omega}{\delta}$ or when $wt = \frac{\pi}{2} - \arctan \frac{\delta}{\omega}$.
A first-order approximation yields,

$$i_\ell)_{max.} \approx \frac{V_o}{\omega\left(\frac{L_s}{s} + \frac{L_c}{n} + L_\ell\right)} e^{-\frac{\pi\delta}{2\omega}} \tag{47}$$

$$P_\ell)_{max.} \approx \left[\frac{V_o}{\omega\left(\frac{L_s}{s} + \frac{L_c}{n} + L_\ell\right)}\right]^2 R_\ell \, e^{-\frac{\pi\delta}{\omega}} \tag{48}$$

A second-order approximation, letting $wt = \frac{\pi}{2} - \frac{\delta}{\omega}$ yields,

$$i_\ell)_{max.} \approx \frac{V_o}{\omega\left(\frac{L_s}{s} + \frac{L_c}{n} + L_\ell\right)} e^{-\delta\left(\frac{\pi}{2\omega} - \frac{\delta}{\omega^2}\right)} \tag{49}$$

$$P_\ell)_{max.} \approx \left[\frac{V_o}{\omega\left(\frac{L_s}{s} + \frac{L_c}{n} + L_\ell\right)}\right]^2 R_\ell \, e^{-2\delta\left(\frac{\pi}{2\omega} - \frac{\delta}{\omega^2}\right)} \tag{50}$$

Equations 49 and 50 can be further simplified for small damping by letting $nC = C_T$ and

$$\omega = \sqrt{\frac{1}{C_T\left(\frac{L_s}{s} + \frac{L_c}{n} + L_\ell\right)}} \tag{51}$$

Then,

$$i_\ell)_{max.} \approx V_o \sqrt{\frac{C_T}{\frac{L_s}{s} + \frac{L_c}{n} + L_\ell}} \; \exp - \frac{\pi}{4} \frac{\frac{R_s}{s} + \frac{R_c}{n} + R_\ell}{\sqrt{\frac{\frac{L_s}{s} + \frac{L_c}{n} + L_\ell}{C_T}}} \tag{52}$$

$$P_\ell)_{max.} \approx V_o^2 \; \frac{R_\ell C_T}{\frac{L_s}{s} + \frac{L_c}{n} + L_\ell} \; \exp - \frac{\pi}{2} \frac{\frac{R_s}{s} + \frac{R_c}{n} + R_\ell}{\sqrt{\frac{\frac{L_s}{s} + \frac{L_c}{n} + L_\ell}{C_T}}} \tag{53}$$

Usually the value of the exponential factor is very close to unity. Making this approximation yields,

$$i_\ell)_{max.} \approx V_o \sqrt{\frac{C_T}{\frac{L_s}{s} + \frac{L_c}{n} + L_\ell}} \tag{54}$$

$$P_\ell)_{max.} \approx V_o^2 \; \frac{C_T R_\ell}{\frac{L_s}{s} + \frac{L_c}{n} + L_\ell} \tag{55}$$

The time integral of the power dissipated in the gas is the energy that is absorbed by the gas. This energy will generate a shock wave if it is deposited in the gas sufficiently fast. The gas will expand shortly after it absorbs energy; subsequent energy that is put into the gas behind the shock wave does not affect the propagation characteristics of the shock

wave. The actual energy in the shock wave would be extremely difficult to calculate but can be expressed as,

$$E_{shock} = \int_0^\infty P_\ell(t)\, g(t)\, dt \tag{56}$$

where g(t) is an unknown function that includes the effects of the expanding plasma in the main discharge.

The effect of shared inductance is to increase the period of the ringing of the current. A simplified case is shown in Figure 4c and the following analysis applies (The impedance Z is the output impedance plus load impedance):

$$Z = j\omega L_\ell + \frac{\frac{1}{j\omega C}}{\frac{1}{1-\omega^2 L_c C} \qquad \frac{1}{1-\omega^2 C(L_1+L_c)}} \tag{57}$$

$$Z = 0 \text{ when } (\omega^2 L_\ell C)(1-\omega^2 C(L_1+L_c)+1-\omega^2 L_c C) = (1-\omega^2 L_c C)(1-\omega^2 C(L_1+L_c)) \tag{58}$$

or when,

$$\omega^2 = \frac{2L_\ell + 2L_c + L_1 - \sqrt{4L_\ell^2 + L_1^2}}{2C\left((L_1+L_c)(L_c+L_\ell) + L_\ell L_c\right)} \tag{59}$$

Consider the special case when $L_1 = L_\ell = 0.1 L_c$ and $C_T = 2C$,

$$\omega^2 = \frac{1}{0.631\, L_c C_T} \tag{60}$$

$$\tau = 2\pi\sqrt{0.631\, L_c C_T} \tag{61}$$

The corresponding period for $L_1 = 0$ and $L_\ell = 0.1 L_c$ is,

$$\tau = 2\pi\sqrt{0.600\, L_c C_T} \tag{62}$$

Therefore, the period of the main discharge is increased slightly by shared inductances.

Mutual inductance in the main discharge circuit can decrease the period of the ringing of the current. The following equations are the result of an analysis of the simplified circuit shown in Figure 4d:

$$\omega = \sqrt{\frac{1}{C_T\left(L_s + \frac{L_c}{2}(1+k)\right)}} \tag{63}$$

$$\tau \doteq 2\pi\sqrt{C_T\left(L_s + \frac{L_c}{2}(1+k)\right)} \tag{64}$$

The coupling coefficient $k = \frac{M}{L_c}$ will be negative for the current flow directions given in Figure 4d. Therefore, for the usual side-by-side placement of condensers (resulting in a negative value for k) the total circuit inductance will be decreased by the mutual inductance between condensers. The resonant frequency is correspondingly increased and the period decreased.

3. Conductors

The design for the conductors that carry the high current in the main discharge circuit is based on the consideration of four problems:
i) the inductance must be a minimum ii) the resistance must be a minimum iii) the conductors must have sufficient mechanical strength to prevent either separation or rupture caused by forces exerted by the current pulse. iv) skin depth effects must be considered.

Both coaxial and coplanar type conductors are in common use in high current discharge circuitry. A third, less commonly used method is to use many parallelled lengths of commercially available coaxial cable (Smith, 1960).

In the driving mechanism used in the present work both coaxial and coplanar conductors have been used. The inductance per unit length for a coaxial conductor when all current is assumed to flow at the facing surfaces of the conductors is,

$$L = \frac{\mu}{4\pi} \ln \frac{r_o}{r_i} \qquad \text{henries/meter} \qquad (65)$$

where μ = permeability of the dielectric, = 4×10^{-7} h./m. for free space, r_o = inner radius of outer conductor, and r_i = outer radius of inner conductor.

When edge effects are neglected the corresponding equation for the inductance of a coplanar conductor is,

$$L = \mu \frac{d}{W} \qquad \text{henries/meter} \qquad (66)$$

where d = conductor separation, and W = conductor width.

It is to be noted that the inductance of two closely spaced conductors could be calculated exactly from a knowledge of the current distribution in the conductors. However, the major component of the total inductance is caused by the current that flows on the facing surfaces of the conductor. Inductances caused by interaction of currents elsewhere in the conductor are of higher value than that caused by the current flowing on the facing surfaces of the conductor. The important point is that all these inductances are in parallel, so the total inductance depends primarily on the one of lowest value - that caused by the close spacing between the inner faces of the electrodes. Also, of course, a more critical treatment would have to include both the skin effect and the fact that less than half the current flows on the inner surfaces.

For low inductance it is apparent that the insulating material between the conductors should be very thin - the separation being determined by the dielectric strength of the insulator. After experimentation with celluloid, polyethylene and mylar for use as an insulating material, it has been found that mylar possesses the best properties. It has less surface leakage than either of the other materials tried, excellent dielectric strength - 6×10^6 volts per centimeter as measured by Imishi et al (1957), and possesses the highly desirable property that it is adhered to by epoxy resin. It has been found that epoxy resin is an excellent high voltage insulator so it has been used extensively in the construction of the high voltage equipment.

The resistance of a conductor to high frequency current is a function of the skin depth (Gray, 1957),

$$\delta = \sqrt{\frac{2}{\mu \sigma \omega}} \qquad (67)$$

where μ = permeability, σ = conductivity, ω = angular frequency.

At a frequency of 200 KC the skin depth in copper ($\mu_R = 1.00$, $\sigma = \frac{1}{1.724} \times 10^6$ mhos/cm. (Hodgman,1954)) is 1.465×10^{-4} meters or 5.77 mils.

The surface resistivity is given by Gray (1957),

$$R_s = \frac{1}{\sigma \delta} = \sqrt{\frac{\omega \mu}{2 \sigma}} \qquad \text{ohms/square} \quad (68)$$

Two times the surface resistivity is the total body resistivity when the skin depth is appreciably less than the thickness of the conductor. For example, the resistance of a copper conductor 1/32 inch thick, 6 inches long and 1 inch wide to a 200 KC sinusoidal signal is due to conduction on

both surfaces and equals $(\frac{1}{2})(R_s)(\frac{6}{1}) = \frac{3}{(1.465 \times 10^{-4})(.59 \times 10^{6})}$

$= 0.347 \times 10^{-3}$ ohms.

Equations 67 and 68 apply when the current is sinusoidal. For a non-sinusoidal current such as that in a damped oscillatory discharge, the solution to the field equations for the fields inside the current-carrying conductor becomes more involved. Gray (1957) analyzes the step and ramp current cases. Levine et al (1958) applies Gray's results to the design of high-current high-frequency conductors. One can use the curves given by Gray to estimate, for example, the field strength at a depth of $x = 10^{-4}$ meters after the first quarter wave of a sinusoidal current of period four microseconds. One can approximate the sinusoidal current by a ramp current that builds up to peak value in one microsecond. The value of the parameter $x\sqrt{\frac{\mu\sigma}{t}}$ is then 0.86 and from the curve given by Gray, the desired value of the field is $H(10^{-4}\,m., 10^{-6}\,secs.) = 0.33\ H(0\,m., 10^{-6}\,secs.)$. The conventional definition of skin depth is that depth at which the fields are attenuated by a factor of 1/e. The same definition applied to the case of a ramp on for one microsecond yields the result that the effective skin depth is about 10^{-4} meters, a value somewhat less than the skin depth for sinusoidal current having a frequency the same as the fundamental frequency of the ramp. At the present frequency of 200 KC., not much evidence of the non-sinusoidal nature of the discharge on the current distribution in the conductors should be noticed. However, at higher frequencies consideration of the pulse nature of the current will be necessary.

Another factor of importance in the design of the conductors is the mechanical force exerted by the currents. Between wires (from Gray,1957),

- to follow page 21 -

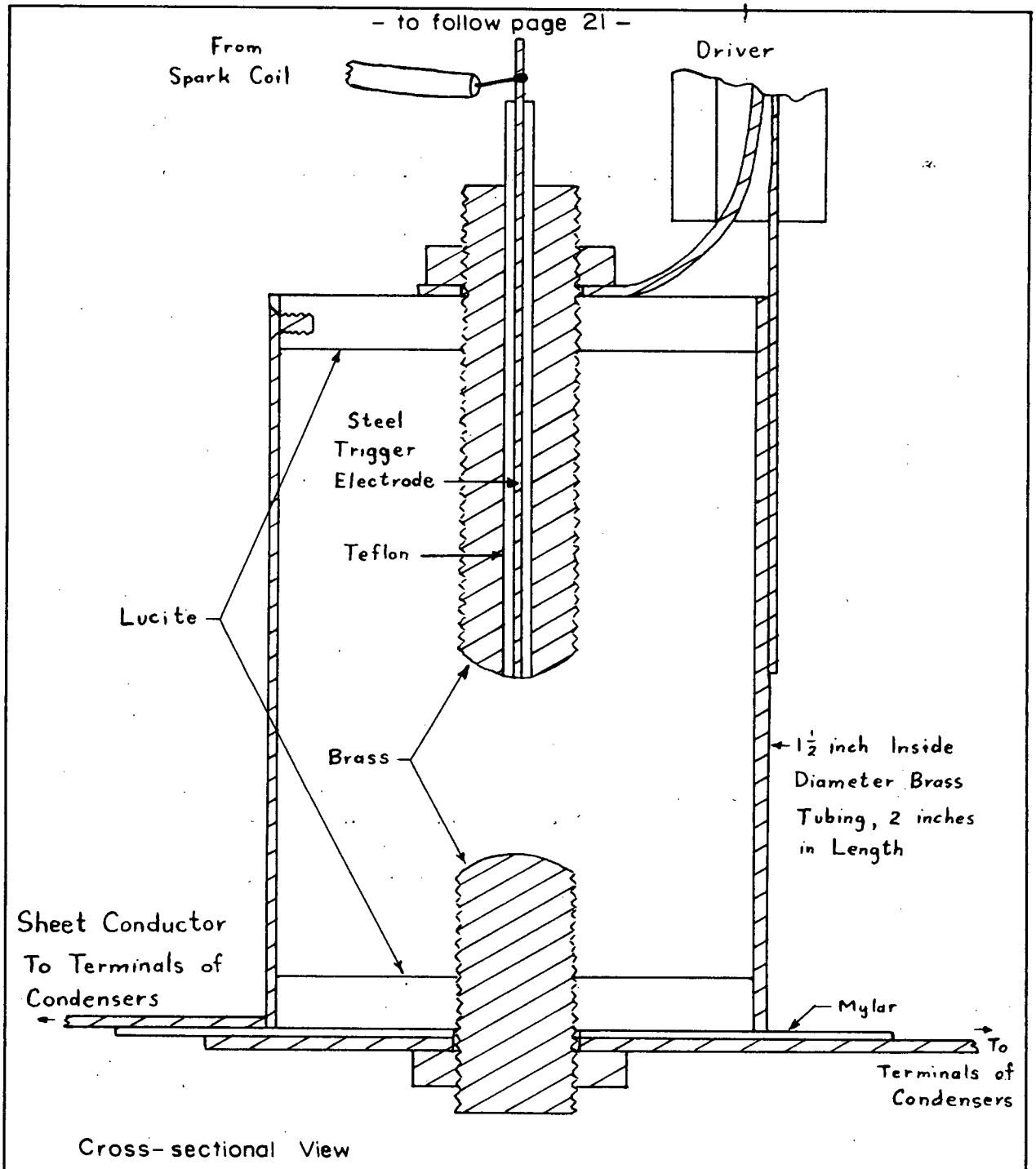

Figure 5 : High Current Switch

$$F = \frac{2\, I_1 I_2}{d} \times 10^{-7} \tag{69}$$

while between coplanar conductors,

$$F = \frac{4\, I_1 I_2}{a}\left[\tan^{-1}\frac{a}{b} - \frac{1}{2}\frac{b}{a}\ln\left(1+\frac{a^2}{b^2}\right)\right] \times 10^{-7} \tag{70}$$

In equations 69 and 70 F is the force in newtons per unit length and is repulsive when the currents I_1 and I_2 flow in opposite directions, d is the separation between the wires, b is the separation between the coplanar conductors, a is the width of the coplanar conductors. For typical values of $a = .0254$ m., $b = 2.03 \times 10^{-4}$ m., $I_1 = I_2 = 65{,}000$ amperes we find from equation 70 that $F = 102{,}000$ newtons/meter = 230 lbs/cm. This force only exists while the current is large, a time of a few microseconds. The physical displacement of the conductors will be governed by the mass and by the method of clamping. A force of 230 lbs/cm. on for a few microseconds can be handled by an extremely weak clamping arrangement.

From equations 42 and 56 it is evident that to obtain maximum current and power in the load the important object in the design of the conductors is to minimize their inductance and resistance.

4. High Current Switch

The main discharge must be turned on with a minimum of switching effects. Both three-electrode spark gaps and ignitrons are popular for this purpose. A three-electrode spark gap has been selected for use on the shock tube driver. The construction is shown in Figure 5 and the inductance can be calculated by considering two coaxial conductors in series of dimensions $r_0 = .0195$ m., $r_i = .009$ m., $l = .038$ m., and $r_0 = .0195$ m., $r_i = .00079$ m., $l = .01$ m. The latter figures apply to the discharge channel, the radius

– to follow page 22 –

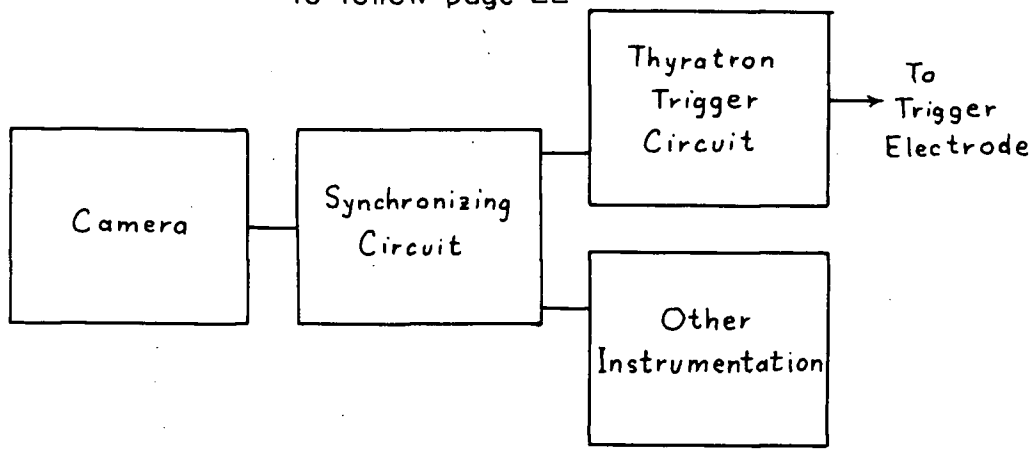

7a : Interconnections

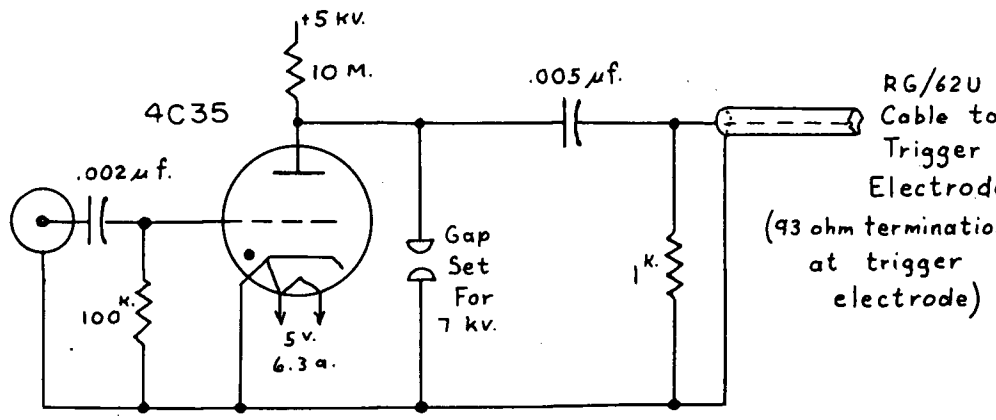

7b : Thyratron Trigger

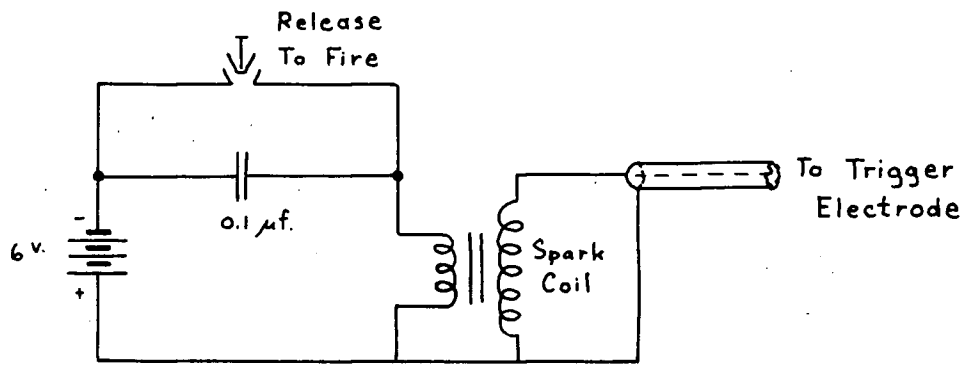

7c : Spark Coil Trigger

Figure 7 : Trigger Circuits

being estimated by visual observation during firing. The total inductance of the switch from equation 65 is, therefore, 6.1 milli-microhenries. The resistance of the switch during conduction is unknown.

5. Trigger Unit

Instrumentation such as a framing camera or a rotating mirror spectrograph will probably necessitate synchronization of the main discharge with some event such as a certain angular position of the mirror in the camera or spectrograph. When such instrumentation becomes available, a suitable synchronizing trigger circuit will be required. The circuit shown in Figure 6 has been designed and built for this purpose.

The synchronizing circuit operates on an input pulse of at least +10 volts from the camera. Within 1.0 ± 0.1 microseconds it sends out a 200 volt pulse suitable for firing the large thyratron in the high voltage trigger circuit (Figures 7a and 7b). The 5 KV pulse from the large thyratron is applied to the trigger electrode of the three-electrode high current switch in the main discharge circuit. The expected time lag between the input pulse and the breakdown of the main switch is 1.5 ± 0.2 microseconds. There has been an alternate output built into the synchronizing circuit that supplies a 200 volt pulse in a controlled time interval after the input pulse is applied of from 3 to 1000 microseconds. The large thyratron can be triggered from either the delayed or undelayed outputs. The unused output of the synchronizing circuit can, of course, be used to trigger other instrumentation. Push-button firing is an alternate mode of operation that has been built into the synchronizing circuit should it not be required to synchronize the firing to the instrumentation.

The interesting electronic features of the synchronizing circuit are: i) The use of a thyratron in the input stage in order to trigger the monostable multivibrator with only one pulse. All of the manual switches that the author has tested for positive closure have been unsuitable because they possessed contact bounce. The effect of such multiple pulses when fed into a monostable circuit makes the operation of the unit unpredictable. The alternative of an electronic switch - a thyratron - was chosen as a suitable driver for the monostable circuit. A second possible circuit which could be substituted for the input thyratron should less time-lag be desired is a binary. ii) The use of a diode clamp and a high pass filter on the delay circuit in the monostable unit. The diode clamp circuit decreases the jitter on the delay and is a commonly used circuit. However, it is believed that the high pass filter in this circuit is an original contribution.

As the need has not yet arisen to use the synchronizing unit, all firings have been triggered with the spark-coil circuit shown in Figure 7c.

6. Condensers

The energy stored in the condensers must be transferred to the load as quickly as possible. From equations 42 and 56 it follows that desirable properties of the condensers in order of importance are: high voltage, high capacity, low internal inductance, low internal resistance.

The internal inductance and resistance are the only two properties that are difficult to measure. The inductance can be obtained approximately by connecting a large cross-section conductor between the terminals and leaving a small gap in the circuit. When the condenser is discharged at gap breakdown voltage, an approximate value for the inductance can be obtained

- to follow page 24 -

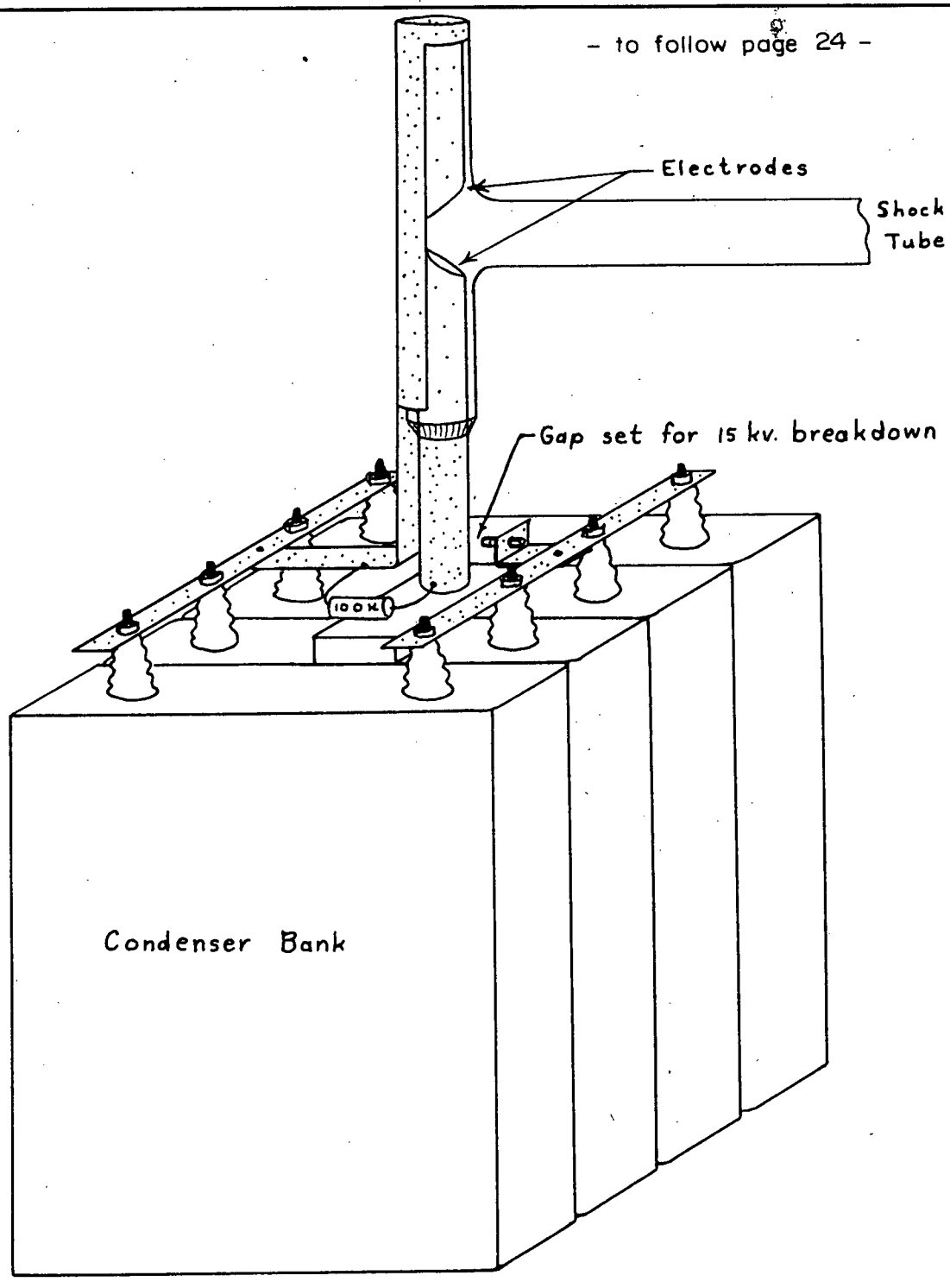

Figure 8 : T-Tube Driver

from the ringing frequency. The internal resistance can be obtained by a similar method by comparing the circuit resistance as determined from the logarithmic decrement of the discharge current waveform with a similarly obtained value when a known low resistance is connected in series with the gap.

The condensers that have been used in the present work are four of General Electric 1 microfarad, 15 KV each having an internal inductance of about 250 milli-microhenries.

7. Electrode System

The object of the design of the electrodes is to obtain a maximum shock velocity for a given condenser energy. The type of electrodes that have been developed in the present work efficiently use the Lorentz force between the currents in the return conductor and the discharge plasma to obtain a high shock velocity.

Initial experiments were performed with the driver shown in Figure 8, which will henceforth be called the T-Tube driver. The electrodes consisted of 3/4 inch diameter brass rods and the return conductor one-half of a split length of 0.1253 inch diameter brass tubing. The distance between the electrodes and the return conductor was about 1/8 inch and was determined by the glass tubing of which the T-Tube was constructed. The inductance of this driver was quite high because of the large spacing between the electrodes and the return conductor. The inductance as determined from the ringing frequency of the current was 330 milli-microhenries. A position-time curve for the luminosity of the shock wave generated by this driver is given in Figure 21 .

- to follow page 25 -

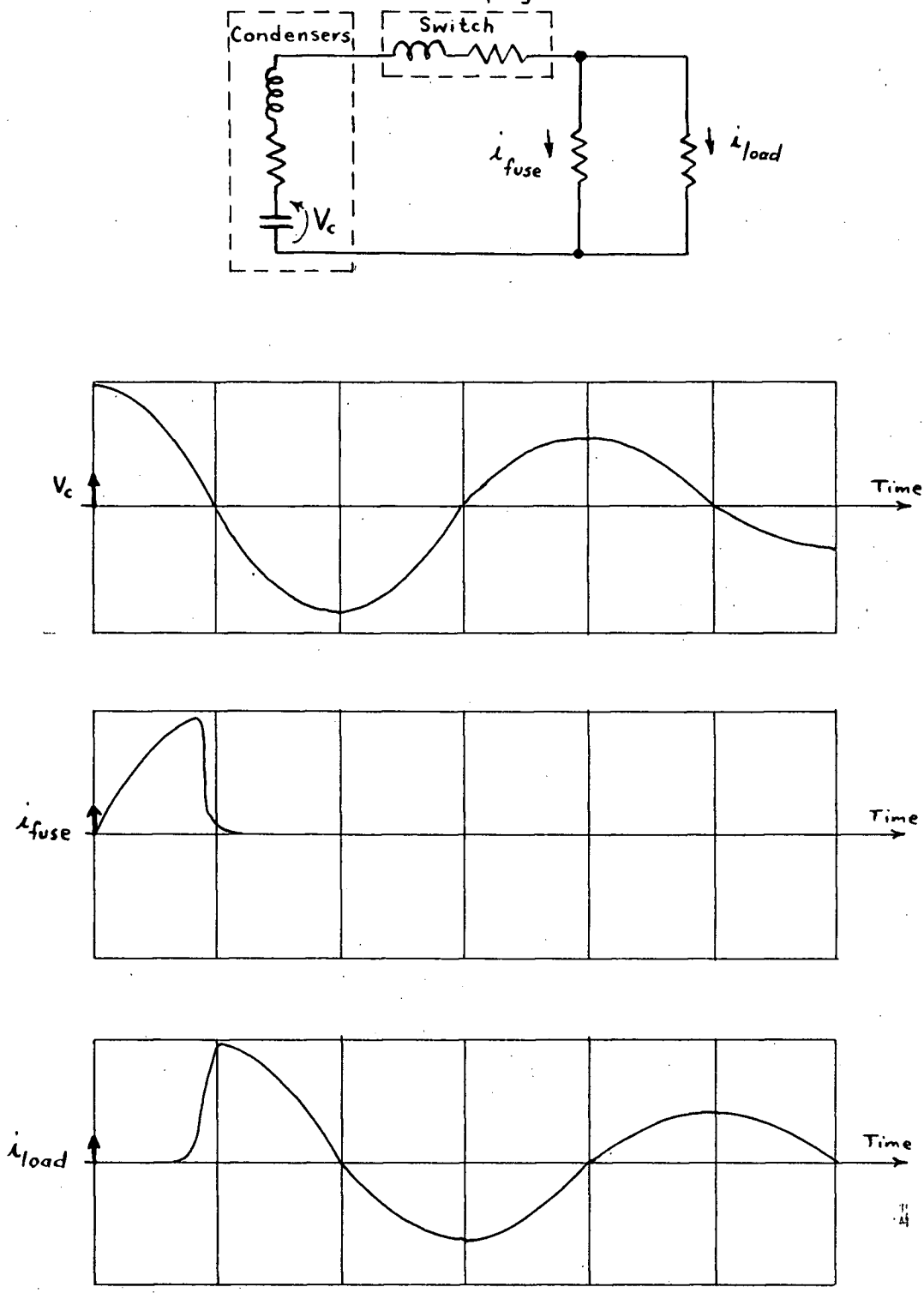

Figure 9 : Current Crowbar

The driving effect of the return conductor was determined by moving it two inches directly back from the discharge chamber. The velocity of the luminosity front decreased from 0.51 cms./microsecond to 0.39 cms./microsecond at a distance of 25.5 cms. from the electrodes when the condensers were discharged from 15 KV. The period as measured from the ringing frequency increased from 7.2 to 8.0 microseconds. The initial energy ($\frac{1}{2}cv^2$) was 450 joules.

The effect on the shock velocity of the spacing between the electrodes was also determined. The result was that maximum velocity was obtained for an electrode spacing of 3.5 cms. between nearest points of the electrodes. This spacing roughly corresponded to that which would offer the smoothest-walled discharge chamber. The curve given in Figure 21 was obtained with this electrode spacing and with the current return conductor tightly clamped to the T-Tube.

The electrodes in the series gap shown in Figure 8 were spaced at such a distance that conduction occurred at a voltage of about 15 KV. The actual firing time of the T-Tube driver was thus somewhat undependable.

An attempt was made to increase the initial rate of use of the current in the main discharge by shunting the base of the electrodes with a "current crowbar". The principle of this method is shown in Figure 9. The current crowbar consisted of a fuse mounted between electrodes spaced further apart than the 15 KV spark breakdown distance in air. The fuse materials considered were, #32 copper wire, 6 ampere strip fuses and 10 ampere strip fuses. The results indicated that the method did not increase the shock velocity because too much power was dissipated in igniting the fuse.

- to follow page 26 -

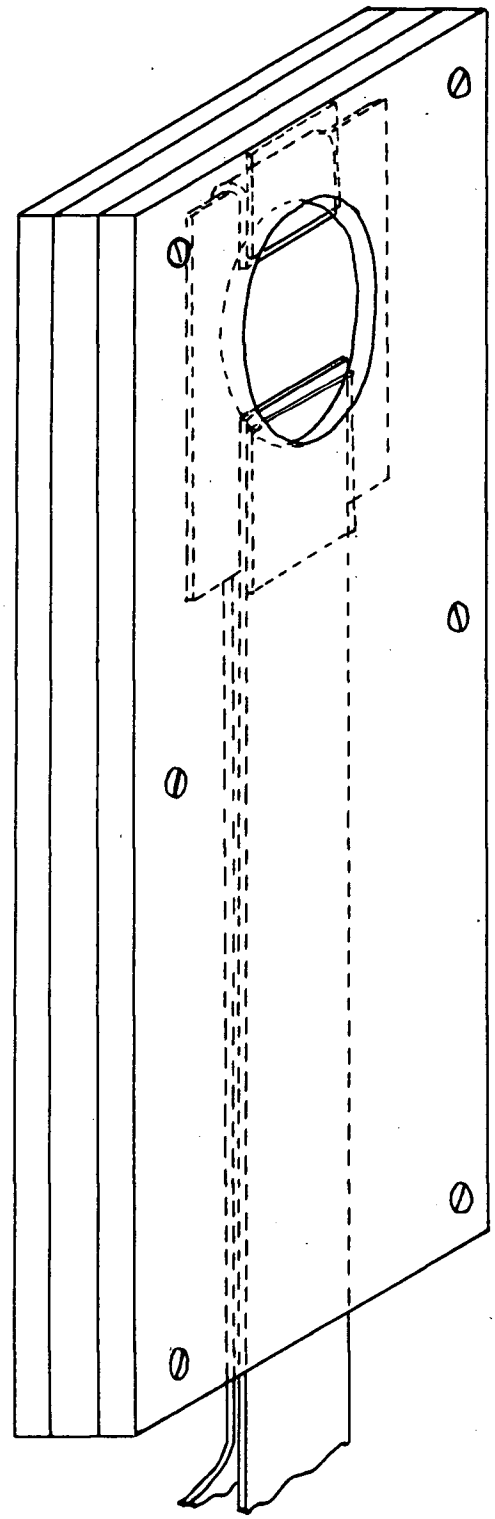

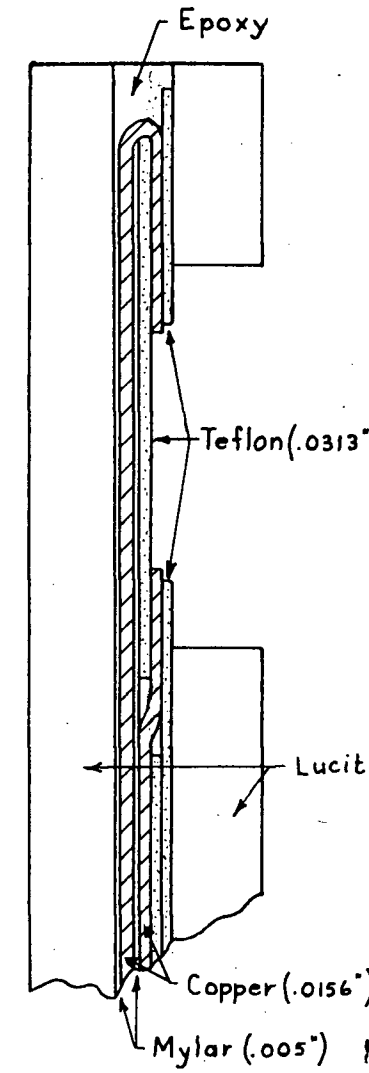

Cross-section Through Electrodes

Figure 10 : Co-planar Driver

The results, however, were promising because they suggest that the method should be of value when the shock velocity is dependent upon the rise-time of the condenser bank. The problem that was not solved but that probably could with considerable more experimentation would be to optimize the fuse ignition time and thermal properties. These properties could probably be optimized by varying the ambient pressure and temperature and the fuse material. Subsequent to the completion of the experimentation just described, a paper was found in which James and Patrick (1958) describe a successful application of this principle.

After some experimentation with the T-Tube driver, it became obvious that a higher shock velocity should be obtained if the inductance of the driver could be decreased. The driver shown in Figure 10 was then developed and subsequently proven to produce a higher velocity shock wave than the T-Tube driver. The development of the coplanar driver was directed toward solving the following problems: i) The main discharge plasma should not contact any material that is easily ablated or changed by high temperatures. This requirement is impossible to meet because the temperature in the main discharge will be at least 400,000°K. However, an approach to a solution to this problem is to use a ceramic material. For ease of construction in the present apparatus, a compromise has been made and teflon used for the high temperature electrical insulator where required. Other methods that have been tried unsuccessfully are, firing aluminum oxide, anodizing and using Sauereisen Insalute cement. ii) The conductors bringing the current to the discharge should have minimum inductance and resistance. The design adopted is to use 10 mil mylar insulation around and between 1/64 inch copper conductors. The dimensions of each of the conductors is about

1 inch by 6 inches, so the inductance and resistance at 200 KC as calculated from equations 66 and 68 is 1.1 milli-microhenries and 0.0028 ohms. iii) The problem of air leaks into the shock tube has been solved by potting the electrodes with the exception of the facing surfaces with epoxy resin. iv) Mechanical forces on the conductors caused by current interaction has been handled by clamping the electrodes together between sheets of lucite. The period of the main discharge current with the coplanar driver connected in the main discharge circuit was 4.5 microseconds. The total circuit inductance was, therefore, 125 milli-microhenries. The maximum current as measured by the method described in Chapter III , Section 9, was 65,000 amperes. The low circuit inductance and high peak current can be attributed to both the design of the coplanar electrodes and the other circuit changes that were added simultaneously. The other changes included the switch described in Section 4 of this chapter and low inductance closely-spaced sheet copper conductors that connected the condensers to the switch. These additions are shown in Figure 10, and Figure 5.

8. Luminosity Detector

The luminosity associated with the shock wave is viewed by two photomultipliers spaced 5 cms. apart along the axis of the tube. Standard photomultiplier circuits are used in this unit. The important characteristics are, 0.2 microseconds rise-time and 3,000°A to about 6,000°A spectral response peaking at 4,000°A (photomultiplier type 931-A). The field of view is determined by adjustable slits inside the box of the detector. For all of the firings the slit widths have been, outer - 0.2 mm., inner - .02 mm. The slit height is fixed at 1.88 cms. The spacing between the outer and inner slits is 15.3 cms. and between the inner slit and the corresponding photomultiplier is 2.5 cms. The field of view is thus 0.3 mm. by 3.6 cm. at the

axis of the shock tube when the outer slits are 8.0 cms. from the axis of the tube. Each photomultiplier in the luminosity detector thus essentially samples the luminosity from a cylindrical volume in the shock tube of dimensions π x tube radius^2 x 0.3 mm. No attempt as yet has been made to make absolute measurements of the intensity of the source emitting the light.

The photomultipliers will overload on the light from strong shock waves. Two methods of readily controlling the sensitivity and thus avoiding overload problems have been adopted: i) neutral density filters (fogged film) have been inserted between the photomultipliers and the inner slits and ii) the dynode voltage has been controlled. The same power supply is used for the photomultiplier in the spectophotometer so that it is often necessary to control the sensitivity of the luminosity detector by the more laborious first method.

9. Current Detector

The current in the main discharge can be determined by measuring the voltage drop across a low known-value resistance that is connected in series with the main discharge. Olsen and Huxford (1952) measured the current in a 4 KV discharge with a 0.053 ohm low inductance resistor.

In the present apparatus the current can reach a peak value of about 65,000 amperes thus creating very large magnetic fields. Because the discharge is oscillatory there also is generated a strong electric field that is 90° out of phase with the magnetic field. The magnetic field generated by the main discharge has been utilized to measure the current thus bypassing

- to follow page 29 -

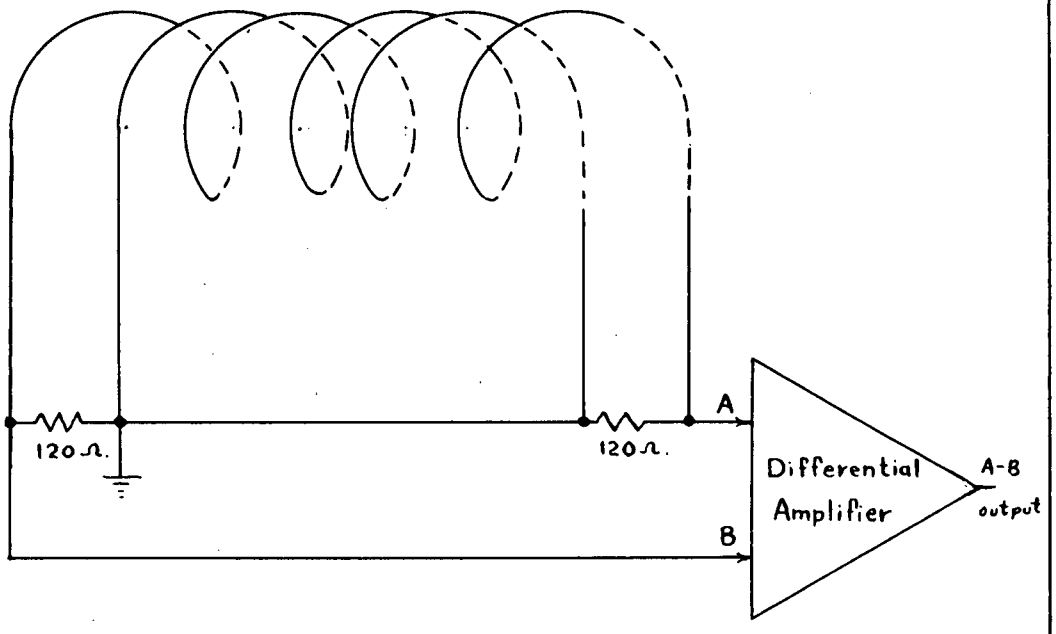

Figure 11 : Current Detector

the problems that would have been encountered should a resistor method have been adopted: i) frequency dependency of the resistance of the resistor (a skin depth problem) ii) spurious signals generated in both the shunt resistance and the voltage measuring cable by the very large fields present and iii) loss of power in the resistor.

The magnetic field generated by the main discharge is measured with two 100-turn coils jumble-wound on a 1/16 inch diameter form with size B & S 36 wire and connected as shown in Figure 11. Connections between the coils and the differential inputs of an oscilloscope were made so that the in-phase voltages (generated by pickup of the electric field) cancelled and out-of-phase voltages (due to magnetic field pickup) added. The capacitance of the connecting cables and the inductance of the coils was such that the 120 ohm resistors gave critical damping to the coils which then had a frequency response flat up to the resonant frequency of 4 mcs. The coils were placed inside the loop formed by the main discharge circuit and oriented so that the axis of the coils coincided with the axis of the loop formed by the main discharge circuit.

The energy stored in the condensers is completely dissipated by a firing. The total charge stored in the condensers is, therefore, equal to the integral of the current flow,

$$\int_0^\infty dQ = \int_0^\infty I\,dt \tag{71}$$

but

$$\int_0^\infty dQ = V_0 C \tag{72}$$

therefore

$$V_0 C = \int_0^\infty I\,dt \tag{73}$$

The observed differential voltage induced across the coils f(t) is given by Faraday's law,

$$f(t) \propto \frac{d\phi}{dt} \tag{74}$$

where ϕ is the magnetic flux which links with the coils. Since the magnetic flux is linearly proportional to the current generating the flux, we have,

$$f(t) = k \frac{dI}{dt} \tag{75}$$

where k is a constant depending on the coil geometry and position with respect to the current-carrying conductors.

Integrating equation 75 and noting that I(o) = 0 yields,

$$I(t) = \frac{1}{k} \int_0^t f(t')\,dt' \tag{76}$$

Equation 73 can now be used to find the value of k. Combining equations 73 and 76 ,

$$k = \frac{1}{V_0 C} \int_0^\infty \int_0^t f(t')\,dt'\,dt \tag{77}$$

Equation 76 will yield the value of I(t) when the value of k as determined from equation 77 is substituted. The value of k will change only when the geometry of either the coil or discharge circuit is altered.

Equations 76 and 77 are extremely general, applicable for determination of the current as a function of time regardless of the shape of the waveform. The coil method for measuring the current is thus applicable to any circuit in which energy of known initial and final value is dissipated sufficiently fast to produce a measurable magnetic field.

When the current waveform is known to be a damped sinusoid and the capacitance and energy change involved is known, then the value of the current can be readily found. The value that is of most interest in the present

apparatus is the peak current - which occurs at the first maximum of the damped sinusoid. For the damped current,

$$I(t) = \frac{V_0}{\omega L} e^{-\delta t} \sin \omega t \tag{78}$$

the observed waveform will be,

$$f(t) = k \frac{dI}{dt} = k I \left(-\delta + \omega \cot \omega t\right) \tag{79}$$

Measurement of the ratio of the amplitudes at two successive maxima of $f(t)$, f_1 and f_2, will give δ ,

$$\frac{f_1}{f_2} = e^{-\delta(t_2 - t_1)} \tag{80}$$

or

$$\delta = \frac{1}{t_2 - t_1} \ln \frac{f_1}{f_2}$$

In practice $t_2 - t_1$ can be obtained more accurately by measurement of the time interval between successive zero values of $f(t)$ rather than maxima.

The value of ω can also be readily obtained from $t_2 - t_1$,

$$\omega = \frac{\pi}{t_2 - t_1}$$

We finally get,

$$I_{max.} = \frac{V_0}{\omega L} e^{-\delta t^*} \sin \omega t^* \tag{81}$$

where

$$\delta = \frac{1}{t_2 - t_1} \ln \frac{f_1}{f_2} \tag{82}$$

$$\omega = \frac{\pi}{t_2 - t_1} \tag{83}$$

$$L = \frac{1}{C(\omega^2 + \delta^2)} \tag{84}$$

$$t^* = \frac{1}{\omega} \arctan \frac{\omega}{\delta} \tag{85}$$

Equations 81 to 85 have been used in the present work to determine the value of the peak current in the main discharge.

– to follow page 32 –

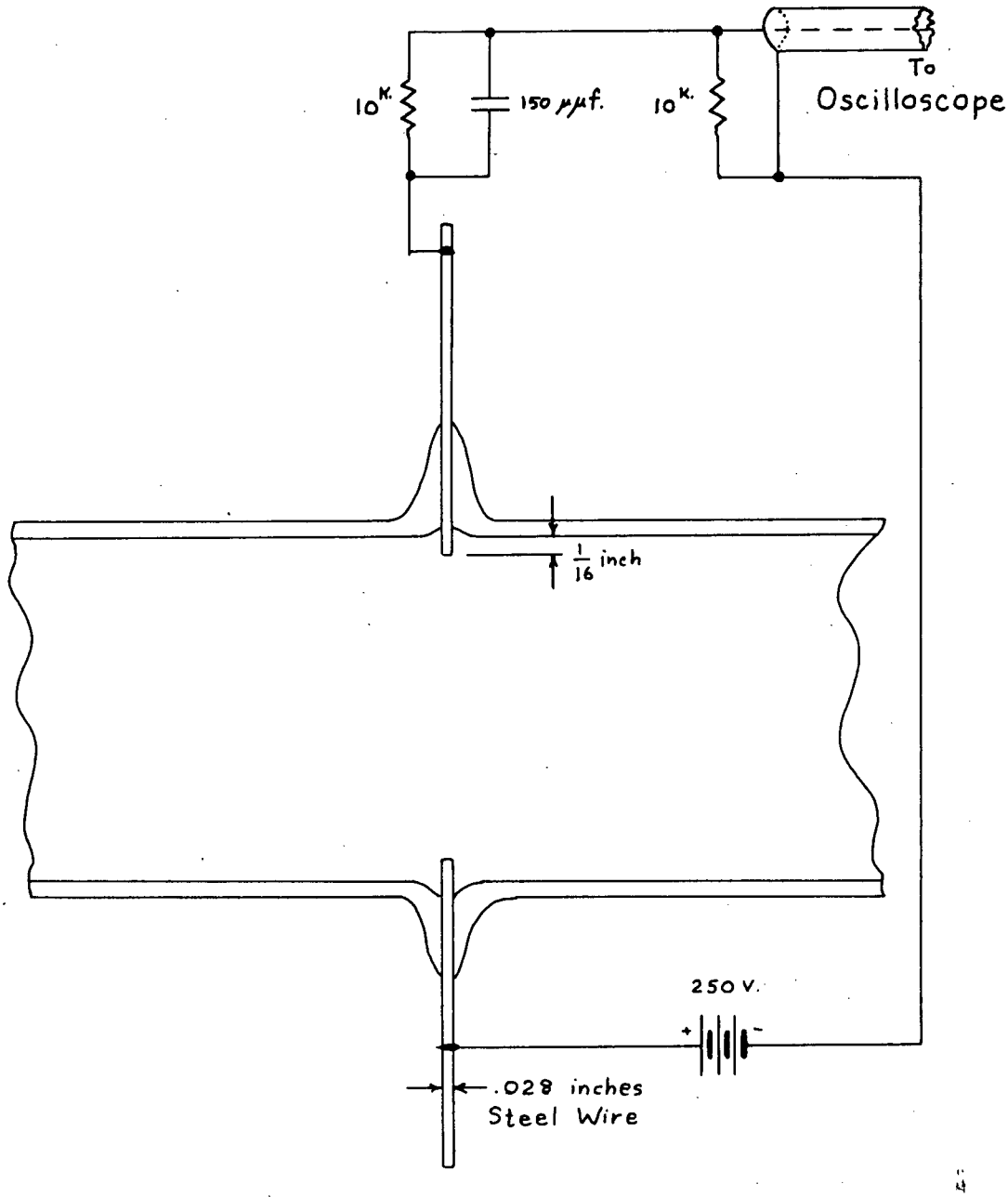

Figure 12 : Electric Probes

10. Voltage Measurements

Very little work has been done by the author to perfect a method for measuring the voltages in the main discharge. The usual method of tapping off the voltage with a resistive attenuator has been tried. The problems of skin effect, and anomalous voltage pickup due to flux linkage with the measuring cables and connections were not tackled. The only problem that was considered was the faithful reproduction of the voltage across a resistive attenuator. A voltage fed into a high resistance (R) in series with a low resistance (r) has a transfer function of the form

$$\frac{E_o}{E_{in}} = \frac{1}{1 + \dfrac{pc + \frac{1}{r}}{pC + \frac{1}{R}}} \tag{86}$$

where c is the total capacity across r, C is the total capacity across R, E_o is the output voltage across r, E_{in} is the input voltage across R + r, and p is the differential operator $\frac{d}{dt}$.

To obtain a frequency independent transfer function the following condition must be met:

$$CR = cr \tag{87}$$

In actual circuit values, R = 100,000 ohms, r = 100 ohms, C = stray capacitance, and c required to give faithful response of a step input voltage was .005 microfarads.

11. Electric Probes

Under special conditions, electric probe studies can yield electron energy distribution, electron temperature (when the velocity distribution is Maxwellian) and a rough estimate of the electron density. Basic probe theory is discussed by Loeb (1955) and Francis (1956).

Electric probes have been used in the present apparatus to measure the conductivity by the same method as used by Lin, Resler and Kantrowitz (1955). Figure 12 gives the circuit details and probe dimensions.

12. Spectrophotometer*

A small Hilger spectroscope has been fitted with an exit slit, a photomultiplier and a cathode-follower. The electronic circuitry is quite standard. The spectral range covered by this unit is 3000°A to 6000°A. The sensitivity of a spectrophotometer is far greater than that of a spectroscope employing photographic plates, so this unit is proving to be a valuable adjunct to the other spectroscopic equipment presently in use. The disadvantage that only a limited spectral range may be viewed at one time is greatly compensated for by the sensitivity and the time resolution obtained. The spectral resolution of this instrument is quite poor, so construction utilizing either a spectroscope or a monochromator having higher dispersion is planned.

13. Time Integrated Spectroscopy

A considerable number of time-integrated spectra have been taken with the spectrograph positioned transverse to the shock tube. Progressively more sensitive and higher dispersion spectrographs have been used. The instrument that has been finally adopted is a Hilger double automatic large quartz and glass spectrograph. The spectral range that has been investigated is 2800°A to 7500°A and both Kodak IIF plates and Ilford HP3 plates have been

* W.V. Simpkinson has been responsible for the construction and operation of this unit.

employed over their respective sensitive spectral ranges. It was found that multiple shots (up to 12) were required in order to obtain sufficient exposure, even when a collimator lens (f/2.0) was used to focus an image of the shock front onto the entrance slit.

14. Apparatus to Measure Conductivity

Considerable effort has been expended to develop a technique to measure the conductivity of the plasma associated with the shock wave. A description of this apparatus would involve a large number of design considerations and is, therefore, postponed to the next chapter.

- to follow page 35 -

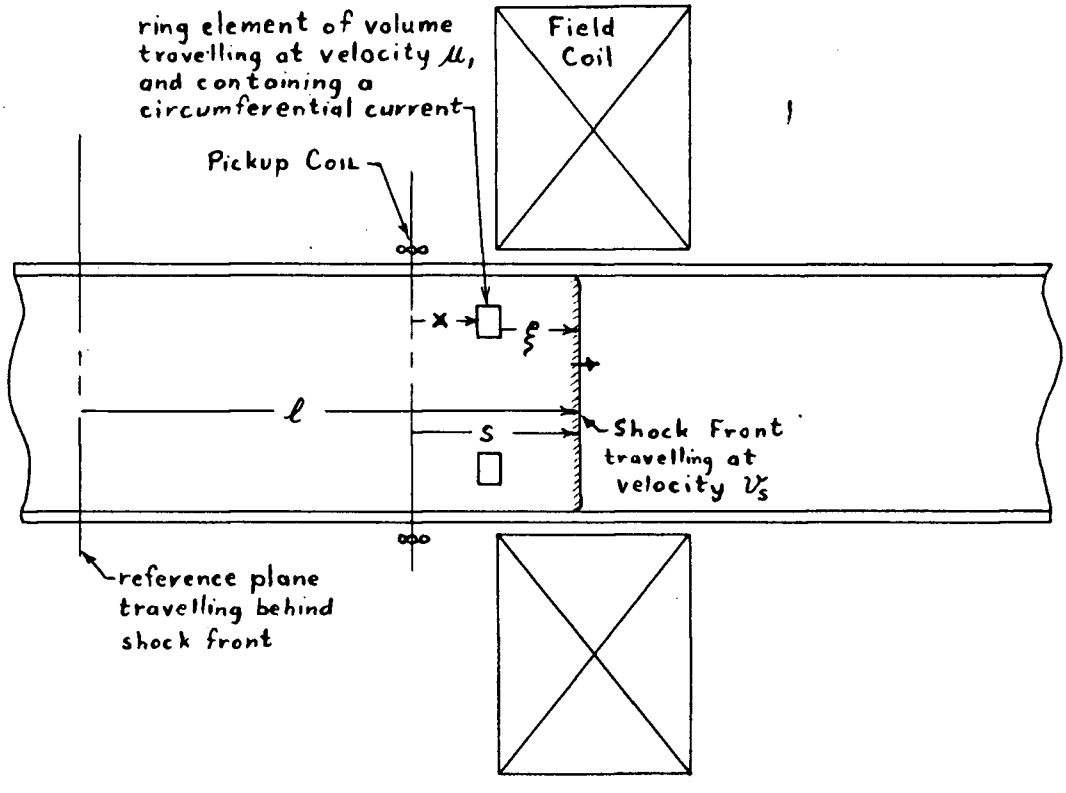

Figure 13: Coordinate System For Conductivity Measurements

IV MEASUREMENT OF THE ELECTRICAL CONDUCTIVITY OF THE PLASMA ASSOCIATED WITH THE SHOCK WAVE

1. Theory

An excellent method of measuring the conductivity of the plasma associated with the shock wave was originally proposed and tested by Lin, Resler and Kantrowitz (1955). The method consists of allowing the shock wave to pass through a radial magnetic field. The $\vec{v} \times \vec{B}$ force on the electrons results in a circumferential current which can be measured by transformer action into a pickup coil. The output voltage from the coil can then be related to the conductivity of the plasma.

The apparatus can be calibrated by one of two methods, either by consideration of all geometric factors or by passing a slug of metal of known conductivity through the coil at a known velocity. The latter method has been employed by the author. The output voltage obtained during calibration as a function of distance $V_c(s)$ can be found from the observed waveform $V_c(t)$ and the velocity of the slug v_c (see Figure 13 for a definition of s and other important distances). The function $V_c(s)$ approximates the Gaussian distribution,

$$V_c(s) = V_{cp} \exp - \left(\frac{s}{b}\right)^2 \tag{88}$$

where b is a length that is characteristic of the resolving power of the apparatus.

– to follow page 36 –

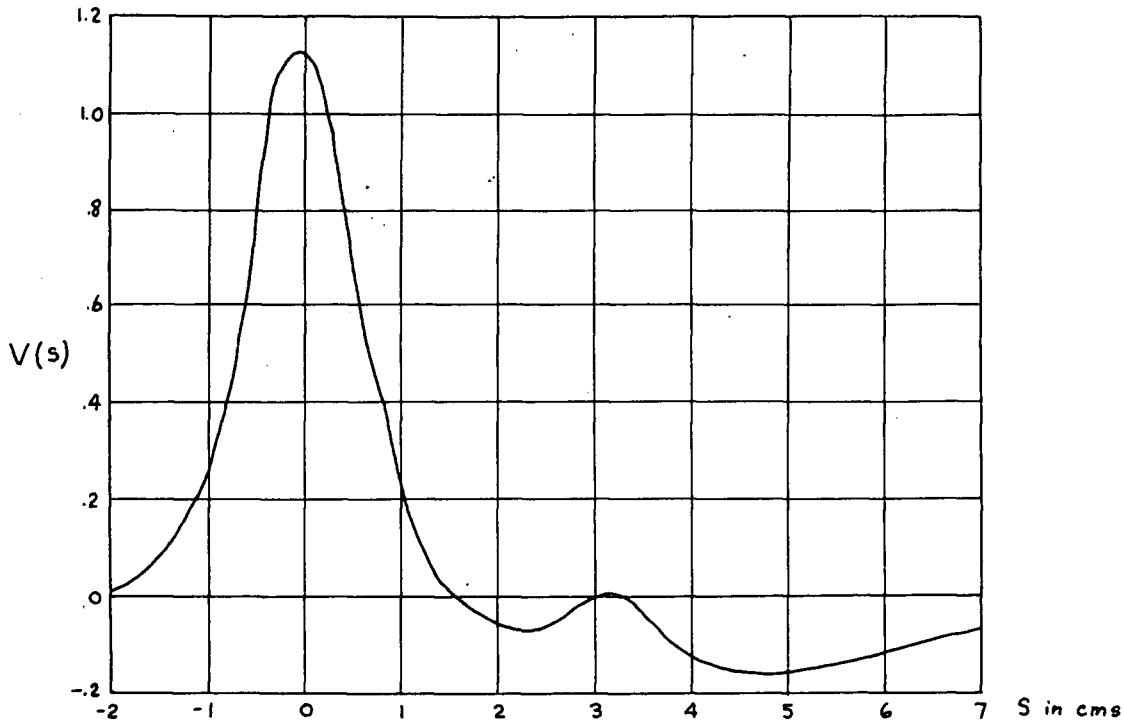

14a : Typical Observed Waveform

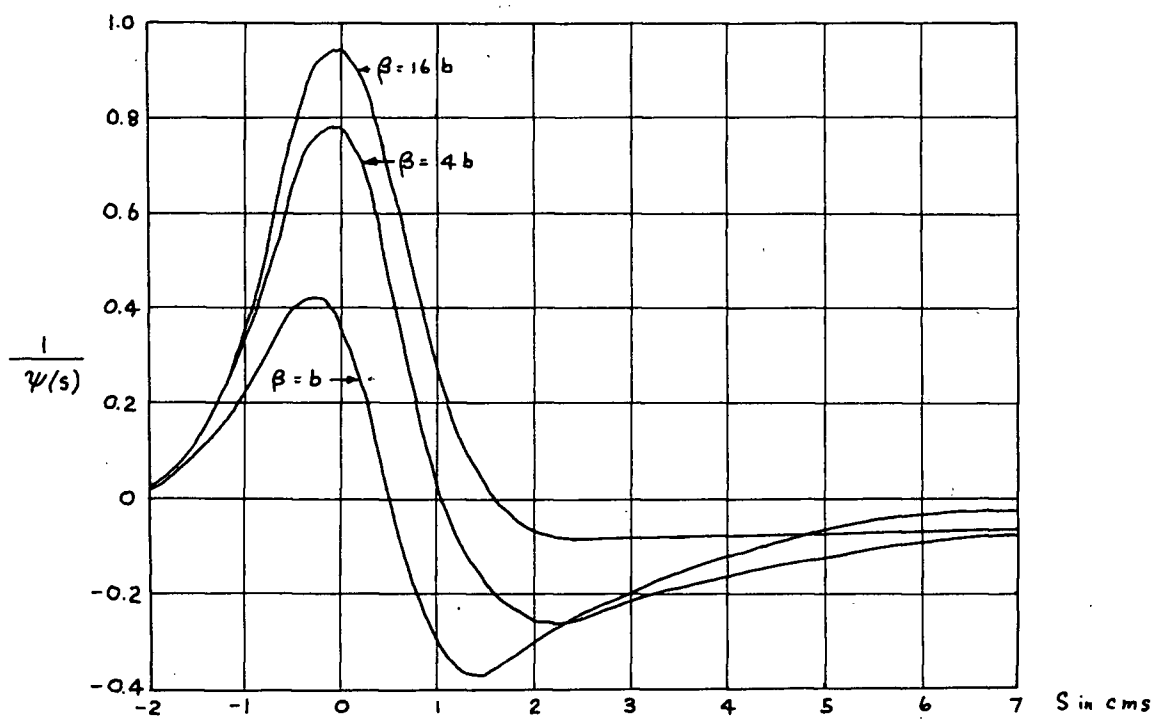

14b : Theoretical Waveforms $\left(\sigma = \sigma^{*} \exp - \frac{s}{\beta}\right)$

Figure 14 : Signals From Conductivity Apparatus

The output voltage obtained during a measurement on the shock wave $V(s)$ can be found from the observed waveform $V(t)$ and the velocity of the ionization front, U, which is very nearly identical to the velocity of the luminosity associated with the shock wave.

Because all of the conductivity measurements on the high temperature gas associated with the shock wave have resulted in $V(s)$ curves that were essentially Gaussian followed by somewhat periodic oscillations (see Figure 14a), it has been concluded that the conductivity very quickly reaches a maximum value and then decays. The rate of decay does not yield much useful information because of the presence of the multiple shocks and field distortion effects to be discussed in Section 2 of this chapter. However, the conductivity as a function of distance over the length of the shock wave must be approximately known in order that the maximum conductivity may be determined.

Lin, Resler and Kantrowitz (1955) derive a relation between the output voltage $V(s)$ and the axial conductivity distribution $\sigma(\xi)$ behind the ionization front through

$$V(s) = \frac{U u_1 I}{v_c^2 I_c \sigma_c}\left\{\sigma(0)V_c(s) - \sigma(\ell)V_c(s-\ell) + \int_{s-\ell}^{s}\sigma'(s-x)V_c(x)\,dx\right\} \quad (89)$$

where u_1 is the flow velocity given by equation 31, I is the current in the field coil during a measurement on the shock wave, I_c that during calibration and σ_c the conductivity of the slug. The method suggested by Lin, Resler and Kantrowitz for determining $\sigma(\xi)$ from equation 89 is to guess at an appropriate function $\sigma(\xi)$ and then calculate $V(s)$ from equation 89. If the correct function $\sigma(\xi)$ has been chosen, then the

calculated V(s) will be identical with the experimental V(s).

A typical experimental curve for V(s) is given in Figure 14a. The shape of this curve suggests that an appropriate $\sigma(\xi)$ function may be,

$$\sigma(\xi) = \sigma^* e^{-\xi/\beta} \tag{90}$$

where $\xi = s-x$

Substituting the following five equations:

$$\sigma(0) = \sigma^* \tag{91}$$

$$\sigma(\ell) = 0 \text{, that is } \lim_{\ell \to \infty} \sigma(\ell) \to 0 \tag{92}$$

$$V_c(s) = V_{cp}\, e^{-\left(\frac{s}{b}\right)^2} \tag{93}$$

$$\sigma'(s-x) = -\frac{\sigma^*}{\beta}\, e^{-\left(\frac{s-x}{\beta}\right)} \tag{94}$$

$$V_c(x) = V_{cp}\, e^{-\left(\frac{x}{b}\right)^2} \tag{95}$$

into equation 89 yields,

$$V(s) = \frac{U\mu_1 I}{v_c^2 I_c \sigma_c}\, \sigma^* V_{cp} \left\{ e^{-\left(\frac{s}{b}\right)^2} - \frac{b}{\beta}\, e^{-\left(\frac{s}{b}\right)} \int_{-\infty}^{\frac{s}{b}} e^{-(y^2) + \frac{b}{\beta} y}\, dy \right\} \tag{96}$$

or

$$V(s) = \frac{U\mu_1 I}{v_c^2 I_c \sigma_c} \left[\frac{\sigma^* V_{cp}}{\psi(s)} \right] \tag{97}$$

where $\psi(s)$ is the reciprocal of the bracketed function in equation 96. The maximum conductivity of the plasma is related to the reciprocal of the maximum of the bracketed function in equation 96. Designating the reciprocal of this value as ψ_1, then,

$$\sigma^* = \frac{v_c^2 I_c \sigma_c}{V_{cp}} \left[\frac{V_p}{U\mu_1 I} \right] \psi_1 \tag{98}$$

where V_p is the maximum value of V(s).

Numerical integration of the bracketed function in equation 96 has yielded the curves given in Figure 14b. These curves are sufficiently close to being identical to the observed V(s) curves (after smoothing out the high frequency oscillations) to warrant their use in data reduction. The value of ψ_1 in equation 98 that has been used during the analysis of the data has been chosen as follows: Each experimental curve V(s) was compared with the curves in Figure 14b. The closest-fitting plotted curve then yielded a value for ψ_1 and a value for β, the logarithmic decrement of the conductivity. Equation 98 could then be solved for σ^*. The fitting has been done with the object of matching the shape of the initial maximum of the experimental $V(s)$ to that of a calculated $V(s)$, noting that the amplitude of the negative portion of the experimental $V(s)$ curve is not dependable. The amplitude of this negative portion will be decreased by the decrease in u_1 (see equations 31 and 98) and will be increased by the field distortion effect to be discussed in Section 3 of this chapter.

It would be desirable to perfect a technique to measure the temperature of the gas behind the shock front as a function of the distance from the shock front. In theory, the conductivity function $\sigma(\xi)$ can be related to a temperature. In the present work no simple theory is very applicable for reasons which will now be discussed. The electrical conductivity of a partially-ionized gas is dependent upon the temperature of the constituents and far less so on the electron density or degree of ionization (at least in the range of temperature and density that is being considered). Therefore, it is believed that maximum conductivity will occur earlier in time than does maximum ionization. Figure 2 is a diagram of the expected relation between the conductivity and the <u>atom</u> temperature behind the shock front. The atom

temperature is neither the same as the electron temperature nor the ion temperature. That is, the plasma being studied is not in thermal equilibrium. The electrons from the ionization by collision reaction (equation 19) are at a lower temperature than the gas atoms so the temperature as calculated from the conductivity measurements (yielding an electron temperature) is expected to be lower than the atom temperature as calculated from the shock velocity. One point to note, however, is that the maximum conductivity will occur at an electron temperature that is considerably higher than the electron temperature that is attained later when equilibrium between the reactions of equations 18 and 19 has resulted in equal ion, atom and electron temperatures. An adequate theory that would relate the conductivity to an electron temperature and then to an atom temperature (providing a check on the atom temperature as calculated from the shock wave conservation equations) is beyond the scope of this thesis.

An approximate value for the electron temperature during maximum conductivity can be calculated from a relation applicable for the conductivity of a fully ionized gas measured transverse to a strong magnetic field and for $T > 8{,}000^{\circ}K.$, as quoted by Spitzer (1956),

$$\sigma = \frac{T^{3/2}}{1.29 \times 10^{4} \ln \Lambda} \quad \text{mho/cm.} \qquad (99)$$

where

$$\Lambda = \frac{3}{2e^{3}} \left(\frac{k^{3} T^{3}}{\pi N_e} \right)^{1/2} \quad \text{for a singly-ionized gas.}$$

The applicability of equation 99 is in doubt because the plasma being considered is neither in thermal equilibrium nor is it fully-ionized. The value of the electron density N_e in the conductivity-temperature

calculations made in this thesis has been taken to be identical to 10^{12} electrons/cm.^{3} This value corresponds to $\alpha = 10^{-4}$ since the atom density in front of the shock front is of the order of 10^{16} atoms/cm.^{3} at the pressures being used. There are two reasons for this choice of a suitable value for N_e. The first reason only imposes logical bounds on the value - which would be $10^8 < N_e < 10^{12}$. The upper bound has been chosen on the basis of the work done by Lin, Resler and Kantrowitz (1955) who on theoretical grounds conclude that a plasma will have a conductivity that is nearly independent of the electron density when $\alpha > 10^{-4}$ and when the plasma is in thermal equilibrium (which it is not in the present case; however this point will not be considered here). Finally, some value for N_e must be chosen in order to use equation 99 . The true value of N_e will be, of course, a function of the temperature of each constituent of the gas, or from another point of view, N_e should be stated as $N_e(\xi)$. It is also to be noted that the choice of a value of N_e does not greatly alter the value for the electron temperature that results from equation 99 because the value of the logarithmic term in equation 99 does not change much even for an order of magnitude change in N_e.

Equation 99 is only valid when the conductivity is measured transverse to a strong magnetic field. One of the criteria of applicability is that the cyclotron frequency (ω) of the electrons must be greater than the electron-electron collision frequency (ν). From Spitzer (1956),

$$\omega = \frac{eB}{mc} \tag{100}$$

For our case, $B_{max.\ axial} = 750$ gauss

therefore, $\omega = 13.2 \times 10^9$ rad/sec.

$$\nu = \frac{\pi N_e e^4}{m^2 v^3} \qquad (101)$$

where N_e = electron density in number per cubic centimeter and v = average electron velocity.

Equating thermal energy to kinetic energy, $\frac{1}{2}kT = \frac{1}{2}mv^2$, neglecting relativistic corrections and substituting in values to obtain the highest possible collision frequency: ($T = 6{,}000^{\circ}K.$, $N_e = 10^{15}$ per cubic centimeter),

$$\nu = 7.4 \times 10^9 \text{ collisions per second.}$$

Spitzer states that the use of equation 101 in calculating the collision frequency in a partially-ionized gas results in a value for ν that is about an order of magnitude too high because this equation has been derived for close encounter collisions only. Electrostatic forces fall off much more slowly with distance than do the forces between neutral particles - upon which equation 101 is based. Therefore, collisions governed by electrostatic forces occur at greater distances and at a lower collision rate than given by equation 101 .

In the present investigation the cyclotron frequency has, therefore, always been greater than the collision frequency during the conductivity measurements and equation 99 is more applicable than the conductivity-temperature relation quoted by Spitzer (1956), for the conductivity of a plasma when a strong transverse magnetic field is not present,

$$\sigma = \frac{T^{3/2}}{6.53 \times 10^3 \ln \Lambda} \qquad (102)$$

- to follow page 42 -

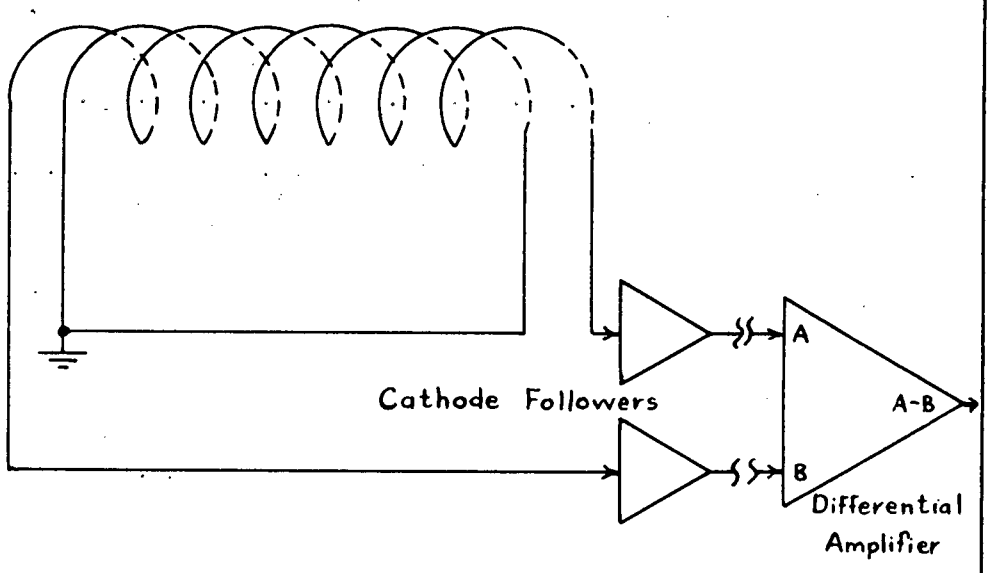

15a : Winding For Best Rejection of Signals Which Are Caused By Electric Fields

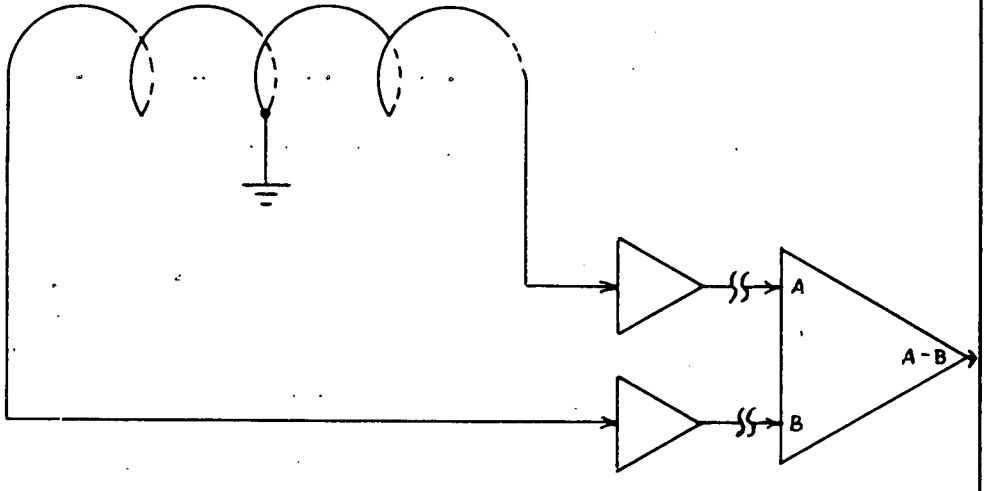

15 b : Winding For Lowest Capacity

Figure 15 : Pickup Coils

It is of interest to calculate typical values for the electron cyclotron radius (r_{cyc}) and the mean free path (L). For T = 6,000°K. (v = .3 x 10^8 cm/sec) and ω = 13.2 x 10^9 rad/sec, then,

$$r_{cyc} = \frac{v_\perp}{\omega} \approx .002 \text{ cms.}$$

$$L = \frac{v}{\nu} \approx .04 \text{ cms.}$$

As the temperature increases both the cyclotron radius and the mean free path will increase. Because the electron cyclotron radius is so much smaller than the dimensions of the shock tube it is strongly suggested that the electrons will follow the field lines and be essentially confined by the field. However, the motion of the ions will be the controlling factor during confinement because neutrality in each increment of volume of the gas will tend to be maintained. Assuming again that T = 6,000°K., then,

$$r_{cyc.}\Big)_{\text{argon ion}} \approx .002\sqrt{\frac{M}{m}}$$
$$\approx 0.54 \text{ cms.}$$

This radius is of the same order of magnitude as the tube radius (1.2 cm.). There thus should be a small confinement effect on the high temperature gas by the magnetic field of the field coils.

2. Apparatus

Lin, Resler and Kantrowitz (1955) employed an 800 turn field coil situated slightly downstream from a pickup coil of 25 turns wound doubly (50 times total) as shown in Figure 15a. It has been found that their technique could be improved by using a pickup coil wound as shown in Figure 15b. This coil has a lower capacitance (due to a lower turn-to-turn voltage) and, therefore, a wider frequency response than the coil shown in Figure 15a. The effect of the method of winding on the capacity was determined by

comparing two coils, one of 39 turns per winding wound as in Figure 15a, and having a capacitance of 24 micro-microfarads, and one of 48 turns per winding wound as in Figure 15b and having a capacitance of 5 micro-microfarads. Low capacitance is needed in order that the frequency response of the coil does not affect the faithful reproduction by the output voltage of the rate of change of flux linking with the coil.

The problem of electric field pickup has been minimized by keeping the length of the pickup coil as small as possible. Number 40 enamelled wire has been used. The in-phase voltages generated in the pickup coil by electric fields will be filtered out by the differential amplifier. An electric field can also cause generation of a differential voltage that is indistinguishable from the differential voltage generated by magnetic fields. An order of magnitude test of the signal with and without the magnetic field on has shown that differential voltages generated by electric field pickup are always between 10 and 100 times smaller than the voltage generated by the magnetic fields. In any case, the signal due to magnetic fields can be separated from that due to electric fields by making observations with and without a magnetic field on.

Two pickup coils have been used. The first is a high sensitivity coil having somewhat poor electrically-generated-differential-voltage rejection characteristics. This coil has 96 turns wound as a single layer as shown in Figure 15b. The length of the winding is 0.8 cm. and the diameter 1.17 inches. The resonant frequency is 7.4 mcs. and the resistance for critical damping 2.2 K. The second pickup coil has low sensitivity but excellent electric field signal rejection characteristics. This coil has a

– to follow page 44 –

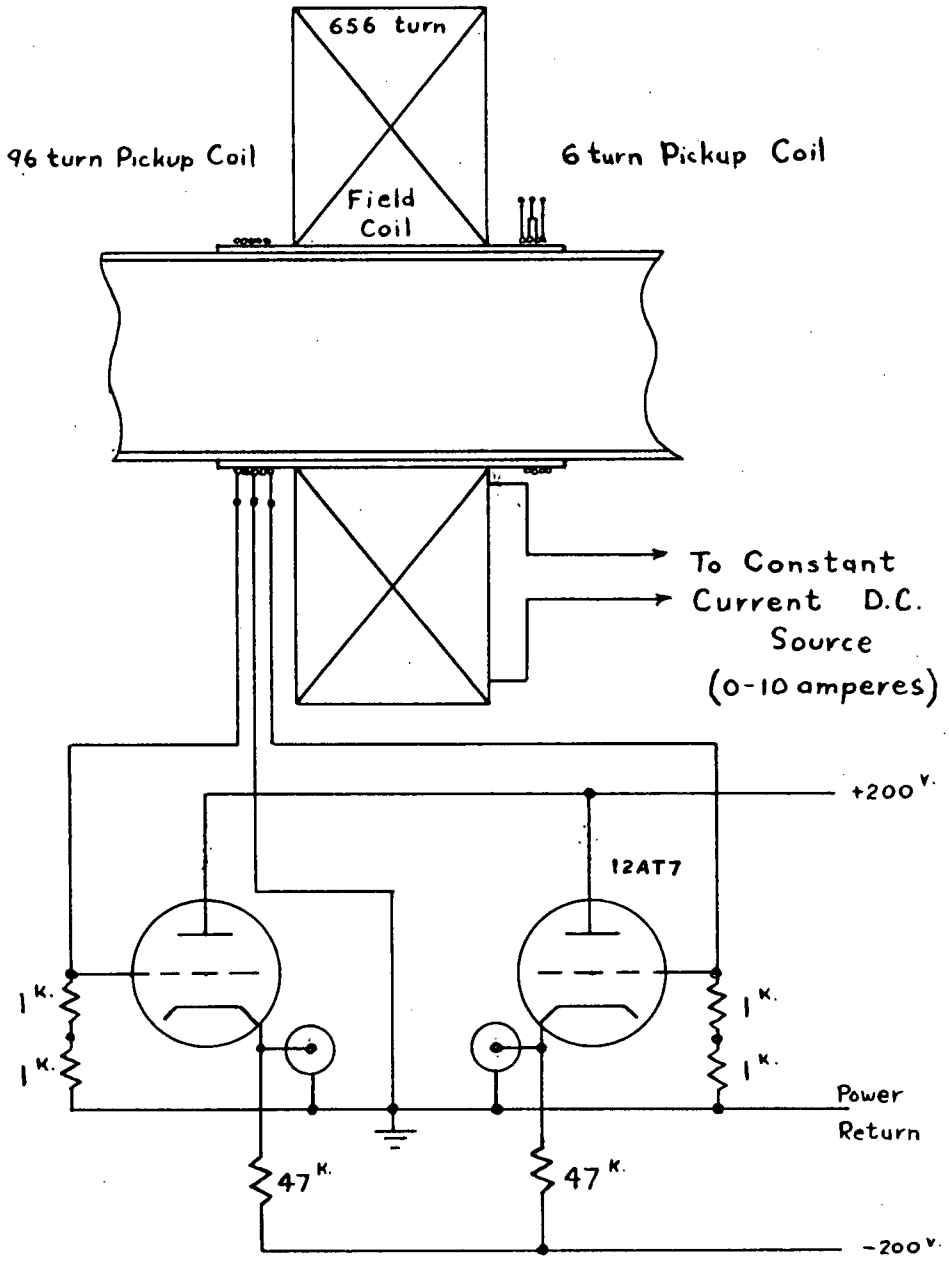

Figure 16 : Apparatus For Measuring Conductivity

total of 6 turns wound as a single layer as shown in Figure 15a. The length of the winding is 0.5 mm. and the diameter 1.17 inches. The same damping resistors have been used with this coil as for the 96 turn coil, so the frequency response up to about 5 mcs. is identical. The 6 turn coil has been used for all measurements that have resulted in a good signal amplitude.

In order to realize the full potentialities of the excellent frequency response of the pickup coils, it was necessary to couple each coil with very short leads to a cathode-follower having extremely low input capacity (circuit is shown in Figure 16). The resulting resonant frequency of the coils of 7.4 mcs. is sufficient to give 96% reproduction of a ramp signal rising to maximum value in one microsecond as calculated by a modification of an equation given by Millman and Taub (1955), (The minimum rise time to maximum value observed for any shock wave signal was 1 microsecond so this time fixed the required high frequency response),

$$\frac{\Delta E_{out}}{E_{in}} = \frac{1}{\pi f T} \qquad (103)$$

for two cascade lag networks and for $\Delta E_{out} \ll E_{in}$, where f = break frequency, T = duration of ramp, E_{in} is the input voltage and ΔE_{out} is the error in the output voltage.

The value of the damping resistance has been calculated from the pickup coil equivalent circuit: a series inductance (L), resistance (r), and voltage generator (E_{in}) shunted by stray capitance C and a damping resistance R,

$$\frac{E_{out}}{E_{in}} = \frac{1}{1 + p\left(\frac{L}{R} + Cr\right) + p^2 LC} \qquad (104)$$

where p is the differential operator $\frac{d}{dt}$

- to follow page 45 -

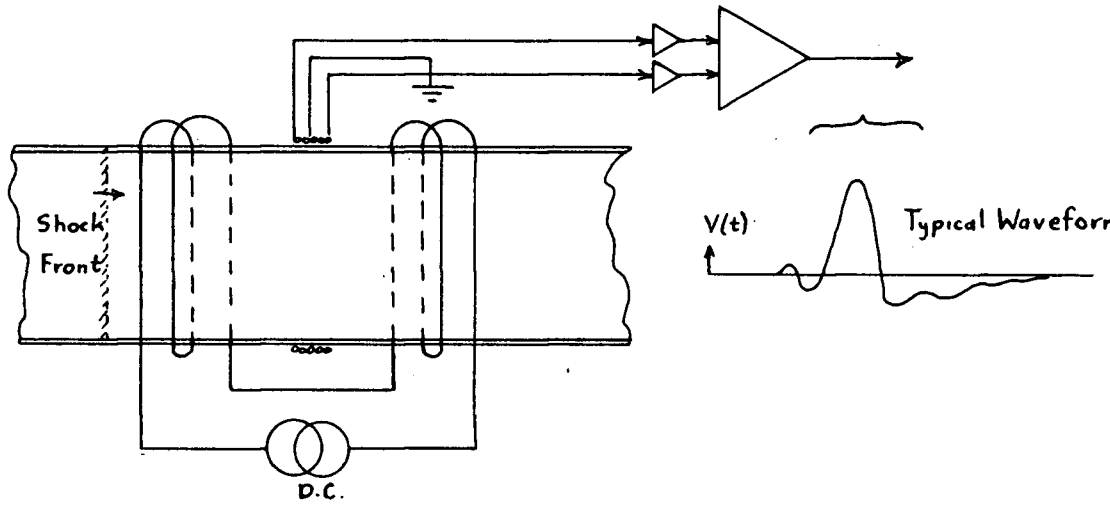

17a : Field Coils Before and After Pickup Coils

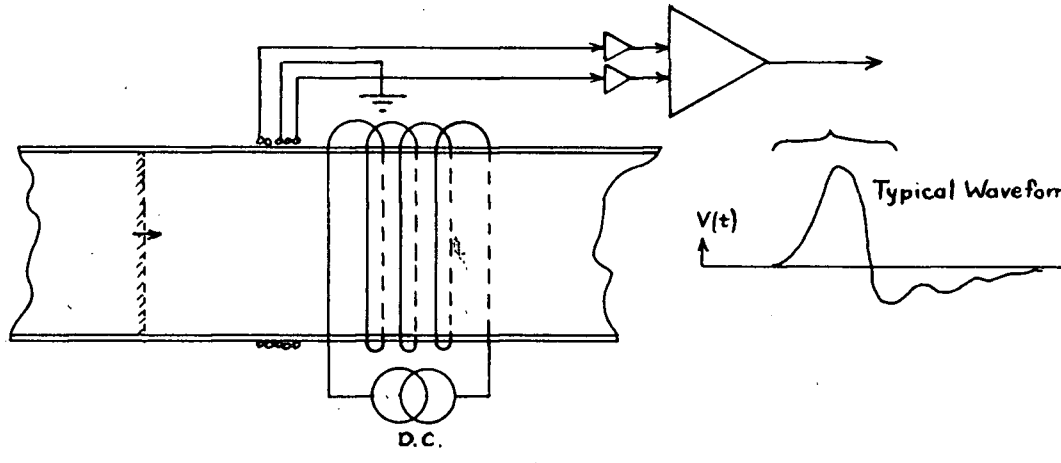

17b : Field Coils After Pickup Coil

Figure 17 : Experimental Evidence of Field Distortion During Conductivity Measurements on Shock Wave

For both the 6 turn and the 96 turn coils the $\frac{L}{R}$ damping term predominates and critical damping occurs when the roots of the denominator in the preceding equation are equal, giving

$$R = \frac{1}{2}\sqrt{\frac{L}{C}} \tag{105}$$

L was measured with a General Radio inductance bridge and C was determined from the undamped natural resonant frequency with the coil connected to the cathode followers. These values when substituted into equation 105 yielded the value R = 2.2 K. for the 96 turn coil. To maintain a good frequency response, the capacitance of this load resistance was decreased by employing for each load resistance, two 1 K. resistors connected in series.

Oscillations are observed following the main signal from the pickup coil as can be seen in Figure 17. It is believed by Lin, Resler and Kantrowitz (1955) that these oscillations were caused by the fundamental mode of radial oscillation of the high temperature gas. The radial oscillation of the gas will cause a voltage to be generated across the pickup coils due to the interaction of the radially-moving charges with the axial field. A theoretical check of this acoustical explanation has been made by consulting Morse (1948) for the radial oscillation equation of a gas in a pipe,

$$p(\phi, r, t) = \begin{matrix}\cos \\ \sin\end{matrix}\, m\phi\, J_m\left(\frac{\omega_n r}{v_{sound}}\right) e^{-i\omega_n t} \tag{106}$$

where $\omega_n = \frac{\pi \alpha_{nm} v_{sound}}{a}$, a is the radius of the pipe, p is the pressure, and $\alpha_{00} = 0$, $\alpha_{01} = 0.586$, $\alpha_{10} = 1.22$, etc.

It is believed that the fundamental mode of radial oscillation would be independent of the angle ϕ when the shock front is planar. For the 10 mode, an initial pressure of 500 microns in argon, a shock velocity of 1.7 cms. per microsecond, a temperature of 260,000°K. immediately behind the shock front ($v_{sound} = .95 \times 10^6$ cms./sec.) and a tube radius of 1.225 centimeters, the radial oscillation frequency from equation 106 is 475 kilocycles per second. The frequency of the fundamental mode of radial oscillation in the region of the shock wave that contains partially-ionized gas would be even lower than 475 kilocycles per second because the velocity of sound in this region would be considerably less than that in the high temperature region immediately following the shock front. The observed oscillations had major frequency components of between 100 and 500 kilocycles per second and, therefore, could be of acoustical origin.

An experimental check on this acoustical explanation for the observed oscillations was made by increasing the ratio of radial to axial magnetic field with the geometry shown in Figure 17a. Should the oscillations following the peak have been due to interaction of the radially moving plasma with the axial field, then the amplitude of the oscillations would depend upon the strength of the axial field. The amplitude of the main peak is dependent upon the strength of the radial field in the vicinity of the pickup coil. Therefore, if the oscillations are of acoustical origin, a change in the ratio of radial to axial magnetic field strength should result in a change in the relative amplitudes of the main peak and the oscillations following the main peak. The experimental waveforms shown in

Figure 17a and 17b indicate that this change was not observed. The observed oscillations were, therefore, not of acoustical origin.

The oscillation that occurs in the signal before the maximum arrives in Figure 17a can be attributed to distortions of the applied magnetic field caused by induced currents in the high temperature gas. Because of this large field distortion effect the double field coil method shown in Figure 17a was abandoned in favour of the single field coil method as used by Lin, Resler and Kantrowitz (1955). It is of interest to note that the double field coils shown in Figure 17a generate a cusped magnetic field. Should the field be sufficiently strong then trapping of the plasma inside the cusped field lines can occur. Scott and Wenzel (1960) discuss the successful trapping of a shock-wave-generated plasma by such a field.

The magnetic field geometry was drastically changed in an attempt to pin down the origin of the oscillations following the maximum. A single turn field coil carrying a current of about 450 amperes was employed. The current was obtained by discharging a condenser bank (2 of General Electric Type 14F97 rated 0.25 microfarads at 50 KV) into the single turn coil at the same time as the main discharge was fired. A suitable inductance (spool of high-voltage cable) was connected in series in order to increase the period of the discharge sufficiently to allow the current through the coil to reach a maximum at about the same time as the shock wave passed through the coils. The current in the field coil was measured by the method discussed in Section 9 of this chapter. A comparison of this signal with that obtained when the 656 turn field coil was employed revealed that the major component of the oscillations was independent of the geometry of the magnetic field.

The conclusion is that the oscillations are primarily caused by a property of the plasma rather than by the magnetic field. It then follows that the plasma associated with the shock wave must have either a non-monotonically-decreasing conductivity function following the initial maximum or that radial oscillations of the plasma exist. It was subsequently verified from observations with the luminosity detector that multiple peaks of luminosity occur at the same times as the conductivity oscillation maxima. Kash et al (1958) have observed similar peaks and have attributed them to the oscillatory nature of the shock driving mechanism. An identical conclusion has been reached in the present work but this point will be discussed later in Chapter V, Section 1. A small component of the oscillations accounting for about 1/10 of the amplitude of the maximum would vary with the geometry of the field. It is believed that this component is caused by field distortion effects. No method is suggested for decreasing this component.

The complete equipment for measuring the conductivity is shown in Figure 16. The field coil finally adopted contained 656 turns of No. 18 enamelled wire having a mean diameter of 6.46 cms., a minimum diameter of 3.15 cms. and a length of 2.83 cms. The axial field strength at the coil center was 125 gauss to 750 gauss for a current input of 1 ampere to 6 amperes. The 6 turn pickup coil has been used for all measurements except when the signal has had an inobservably small amplitude due to a low shock velocity.

3. Calibration

To calibrate the conductivity apparatus a slug of copper, 6 cms. long, was dropped through the field coil, its fall being guided by a glass tube.

This method had the advantage that the velocity could be readily controlled and measured.

In the present investigation the skin effect must be taken into account in the interpretation of the conductivity measurements. Lin, Resler and Kantrowitz did not encounter this problem because they were concerned with lower velocities and conductivities. A rigid solution of the field equations to determine the magnitude of the skin effect would be extremely difficult. However, when

$$\sigma^* U = \sigma_c v_c \tag{107}$$

the skin effect would be almost identical during calibration and during measurements on the shock wave. (This is true insofar as we can consider the plasma as a slug of constant conductivity σ^* moving with velocity U). In order to see that equation 107 is valid, consider the simpler one-dimensional problem of a slug moving into a field increasing linearly with distance.

For a copper slug moving at velocity v_c into a field,

$$H(x=0, t_c) = C x^* \tag{108}$$

where $x^* = 0$ when $t_c = 0$, x is the moving coordinate that is measured into the slug from the front face, and $x^* = v_c t_c$, the field inside the copper is given by Gray (1957) as

$$H_{Cu}(x, t_c) = C x^* f\left(x\sqrt{\frac{\mu\sigma_c}{t_c}}\right) \tag{109}$$

where μ is the permeability of the copper.

For a slug of plasma moving at velocity U into the same field, noting that $x^* = U t_p$, the field inside the plasma is

$$H_p(x, t_p) = C x^* f\left(x\sqrt{\frac{\mu\sigma^*}{t_p}}\right) \tag{110}$$

The relation has been used that,

$$v_c t_c = U t_p \tag{111}$$

Substituting equation 107 and 111 into equation 110 yields,

$$H_p(x, t_p) = c x^* f\left(x \sqrt{\frac{\mu \sigma_c}{t_c}}\right) \tag{112}$$

or,

$$H_{Cu}(x, t_c) = H_p(x, t_p) \tag{113}$$

The field pattern inside the copper slug is, therefore, identical to the field pattern inside the slug of plasma when the slugs have penetrated equal distances into the field. Because the skin effect is governed by these field patterns, we can conclude that the skin effects are identical in this simplified case. We cannot conclude that skin effects are identical when equation 107 is satisfied if we consider the real case of three- dimensional diffusion of fields into a slug. We can only conclude that skin effects should be almost identical when equation 107 is satisfied.

The problem of skin effect can be considered from the point of view of the magnetic Reynolds number (R_M). The magnetic Reynolds number is a measure of the domination of the transport of field lines by a conductor moving with respect to a magnetic field over the leakage of field lines into the conductor. Cowling (1957) defines R_M as follows:

$$R_M = \frac{L v}{\eta}$$

where L is a characteristic length of the flow, v is the velocity of the flow and $\eta = (4\pi\mu_R\sigma)^{-1} \times 10^9$ with μ_R = relative permeability = 1 for a plasma and σ = conductivity of the plasma in mhos per centimeter.

- to follow page 51 -

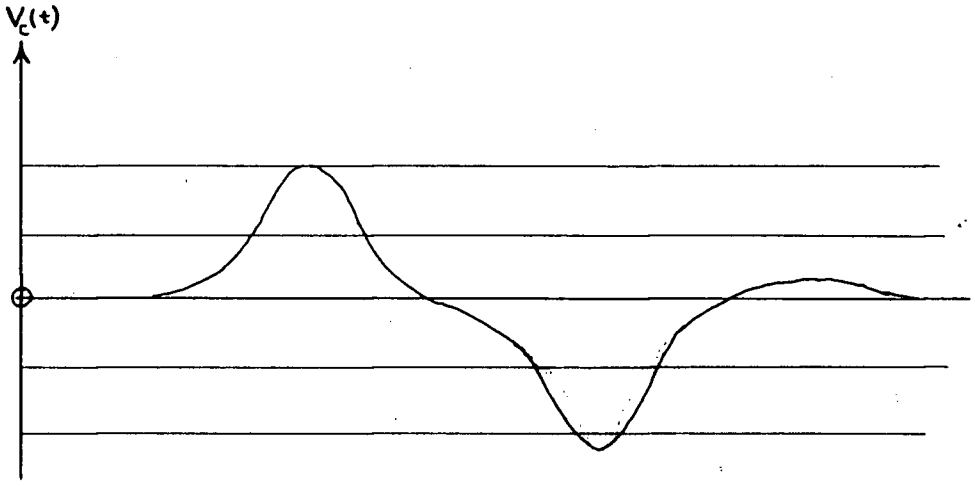

18a : Typical $V_c(t)$ Waveform

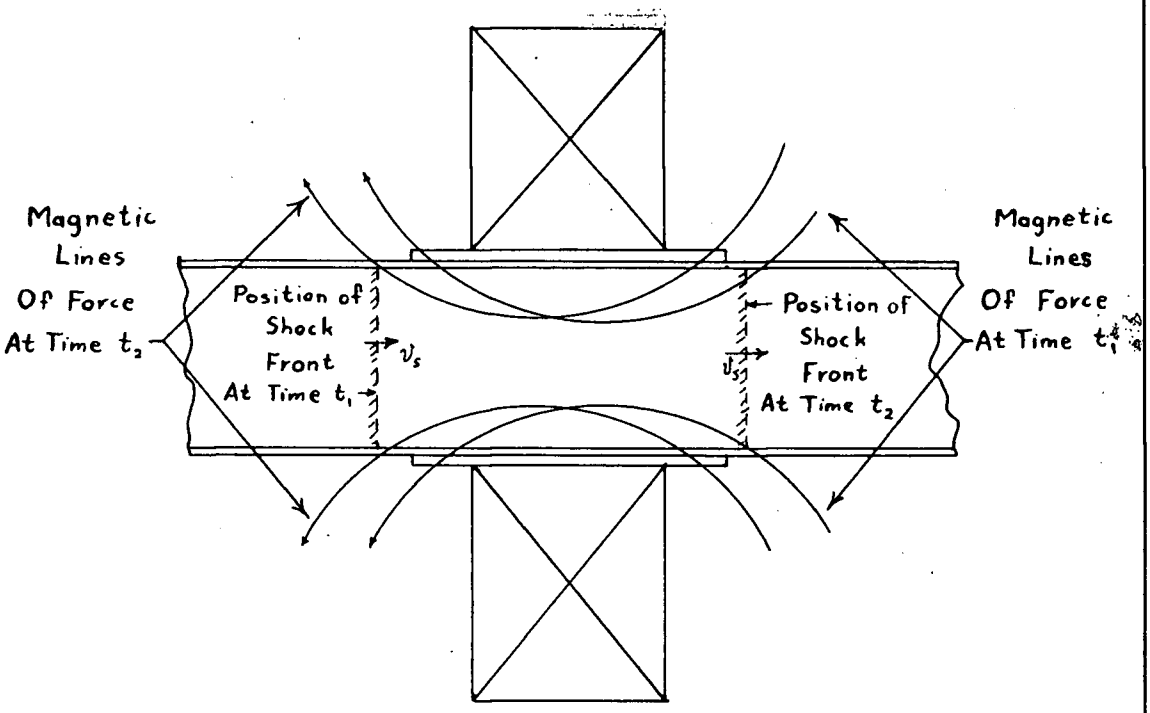

18b : Field Distortion

Figure 18 : Distortion of Magnetic Field During Conductivity Measurements

Thus for a typical value of $\sigma v = 42 \times 10^6$ mhos per second and $L = 1.2$ centimeters, we find $R_M = 0.6$. Again for $\sigma v = 250 \times 10^6$ mhos per second, $L = 1.2$ centimeters, $R_M = 3.8$. Since R_M is of the order of unity we can conclude that a considerable amount of the magnetic field due to the field coil is transported inside the moving specimen.

The skin effect can also be considered from the point of view of the distortion of the magnetic field of the field coils which is caused by induced currents in the specimen. The second peak observed during calibration has been consistently about 10% larger than the first peak (Figure 18a). Also, a small signal is always generated after step changes in conductivity (Figure 18a). Both of these observations can be attributed to distortion of the main field by the field produced by circumferential currents generated in the specimen when it reaches the downstream side of the field coil. This field distortion effect is shown in Figure 18b. The small signal that is generated after step changes in conductivity is also shown in the calibration signal given by Lin, Resler and Kantrowitz (1955), but they do not discuss this. It was first believed by the present author that the increase in the height of the second calibration peak over the height of the first peak was due to a higher velocity of the specimen when it was leaving the pickup coil than when it was entering. However, as a free fall drop of the specimen was being used during calibration, the equations of motion for the specimen could be readily solved to give the velocity of the specimen when it entered the pickup coil and when it left the coil. The increase in velocity that would explain the increase in signal amplitude corresponded to an acceleration of at least 1800 cms./sec^2, an impossibly high value.

The alternative explanation for the signal amplitude increase - that the field was distorted by the slug - is more plausible. Resler, Lin and Kantrowitz (1955) could have neglected this distortion effect because the method that they employed to drive the slug through their apparatus, a rubber-band drive, could easily result in sufficient deceleration over the length of the specimen (a lower velocity at the trailing end would result in a smaller signal) to compensate for the field distortion effect (which would result in a larger signal when the trailing end passed through the pickup coil). Another effect noted that supports the suggestion that there is distortion of the main field is that the amplitude of the signal caused by the trailing edge was consistently larger than that caused by the leading edge when the slug was allowed to slide through the coils at an angle. When the sliding distance is kept constant while the angle is varied, the acceleration of the slug while passing through the coil will decrease. This decrease in acceleration should result in a decrease in the ratio of the peak amplitudes of the signal if the peak amplitudes depended only on the velocity. The experimental result was that the trailing edge peak was still about 10% higher than the leading edge peak. Therefore, field distortion due to currents in the specimen can cause about 10% error in the signal from the pickup coil.

An experimental approach to the problem of skin effect has revealed that $V_c(s)$ approximates a Gaussian distribution function when σ_c is a step function (that is, during calibration). The value for b, as closely as could be determined, is independent of the skin-effect parameter over the range of 42×10^6 mhos per second $< \sigma_c v_c <$ 250×10^6 mhos per second.

This range of $\sigma_c v_c$ corresponds to the range expected of $\sigma^* U$. Also, V_{cp} is, as closely as could be determined, independent of the skin effect over the same range of $\sigma_c v_c$. The skin depth that corresponds to a value of $\sigma_c v_c = 250 \times 10^6$ mhos per second can be calculated from equation 67 noting that ω is approximately $\frac{\pi v_c}{2b}$. This relation is based on the assumption that the Gaussian distribution may be approximated to by one peak of a sine wave. The resulting skin depth is then 0.6 centimeters.

The conductivity measurement apparatus was calibrated by passing a cylindrical slug of copper 6 centimeters in length through the coils at a known velocity. The average velocity was determined by measuring the time lapse between the signals due to the leading edge of the slug passing through the coil and the trailing edge passing through the coil. A first order correction determined from the ratio of the maximum amplitudes (after a correction factor had been included to compensate for the field distortion effect discussed in the preceding paragraphs) was applied to this average velocity to obtain the velocity when the slug entered the coil. The amount of this correction to the velocity was always less than 5%. The values of b and $\frac{I_c v_c^2}{V_{cp}}$ for the signal generated by the leading edge of the slug and obtained from an average of many runs taken over the range of 42×10^6 mhos per second, $< \sigma_c v_c < 250 \times 10^6$ mhos per second was:

Pickup Coil	b in cns.	$\frac{I_c v_c^2}{V_{cp}}$ in amperes cm^2/sec^2 volt
6 turn	1.03	225×10^6
96 turn	1.02	12.7×10^6

TABLE I: CALIBRATION DATA FOR CONDUCTIVITY APPARATUS

Only the signal generated by the leading edge of the slug was considered in the determination of b and $\frac{I_c v_c^2}{V_{cp}}$ in order to approximately match the skin effect errors that occur during calibration and during measurement of the conductivity of the shock wave.

The value of σ_c was found by measuring the voltage drop between two axially-separated cross-sections of the slug when a direct current was passed through the slug. The result was $\sigma_c = 0.581 \pm .006 \times 10^6$ mhos/cm.

To determine the effect of a possible separation of the high temperature gas from the walls of the shock tube (caused by either cooling of the high temperature gas by the walls or partial confinement by the magnetic field), a comparison was made of the signals that resulted when three slugs of different radii were passed through the apparatus. The slug that was employed to obtain the data in Table I had a diameter of 2.45 mm, approximately .005 mm less than the inner diameter of the shock tube. The smaller diameter slugs were increased in diameter to 2.45 mm with cellulose tape in order to ensure that the slug would pass through the coils symmetrically. For equal velocities for three slugs having different diameters, the signal amplitudes were: i) diameter = 2.45 mm, V_{cp} = 1.00 volt, ii) diameter = 2.40 mm, V_{cp} = 0.93 volt, iii) diameter = 2.35 mm, V_{cp} = 0.83 volt. The conclusion is that should the plasma associated with the shock wave be separated from the walls of the shock tube, then the observed signal will be anomalously small.

- to follow page 55 -

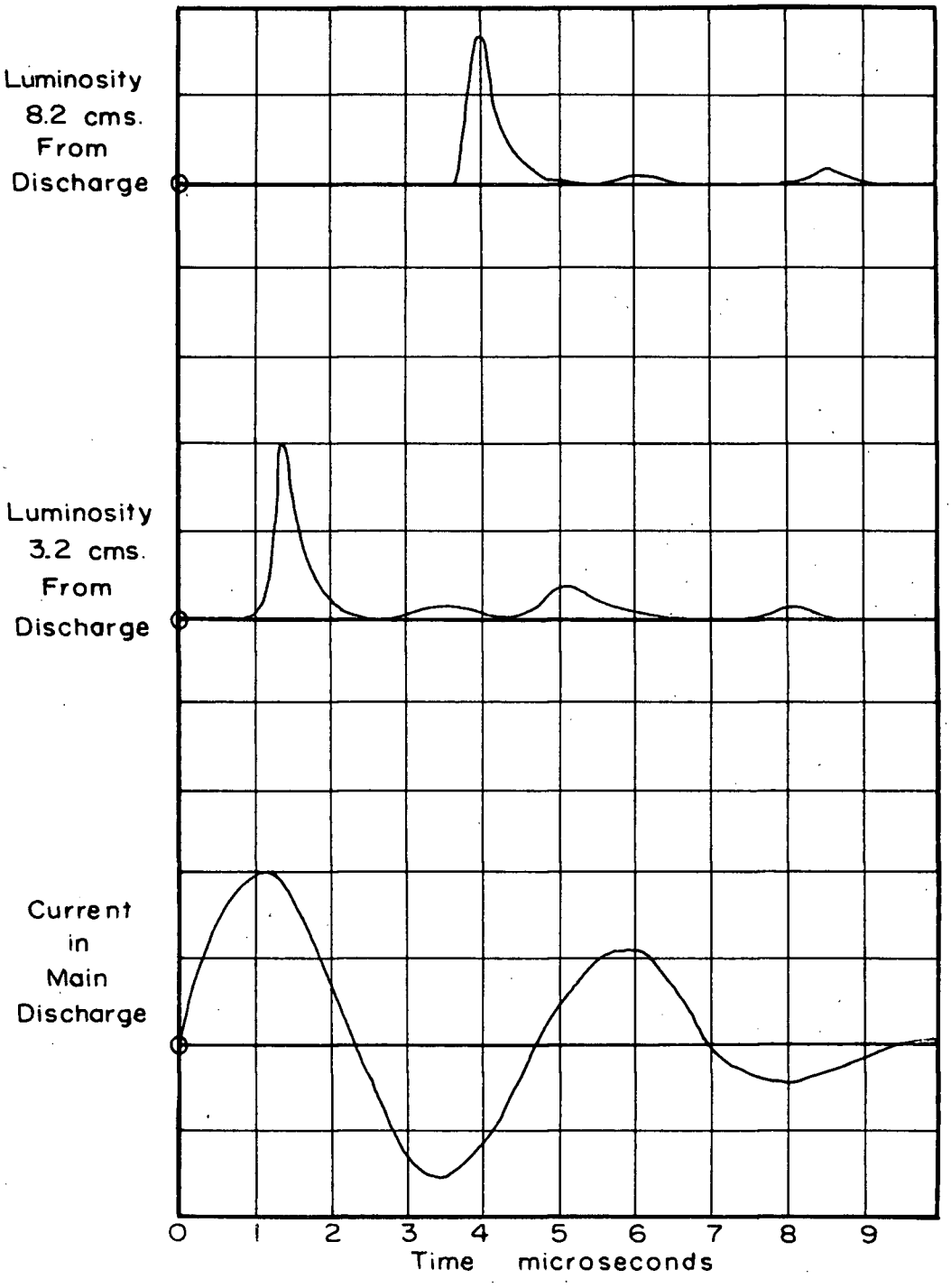

Argon, 500 microns initial pressure, co-planar driver

Figure 19 : Luminosity of Shock Wave

V RESULTS

1. The Shock Driving Mechanism

No author has yet definitely stated what properties are most desirable in the driving mechanism. Klein and Brueckner (1960) come the closest to this problem - they consider the kinetics and driving requirements for a plasma ionized and driven by the magnetic field of a pulsed current in a coil surrounding the plasma.

Measurements with the luminosity detector close to the discharge have shown that there are multiple shock waves generated by the coplanar driver. The initial shock front can be attributed to the energy that is transferred into the gas over approximately the first half cycle of the power dissipated in the gas. The energy that is transferred into the gas during the second half cycle of the power generates a second shock wave. It is probable that an explanation for this double shock characteristic is that there is a space and time dependent current path in the discharge chamber that at first transfers energy into the initial shock front and then, as the initial shock front moves away from the electrodes, this energy is dissipated in a lower impedance path closer to the electrodes that results in the generation of the second shock front. Subsequent shock fronts are generated by each maximum of the power. The luminosity of the entire shock wave that is generated is shown in Figure 19 along with the corresponding current waveform. These curves can be interpreted to yield a rough

- to follow page 56 -

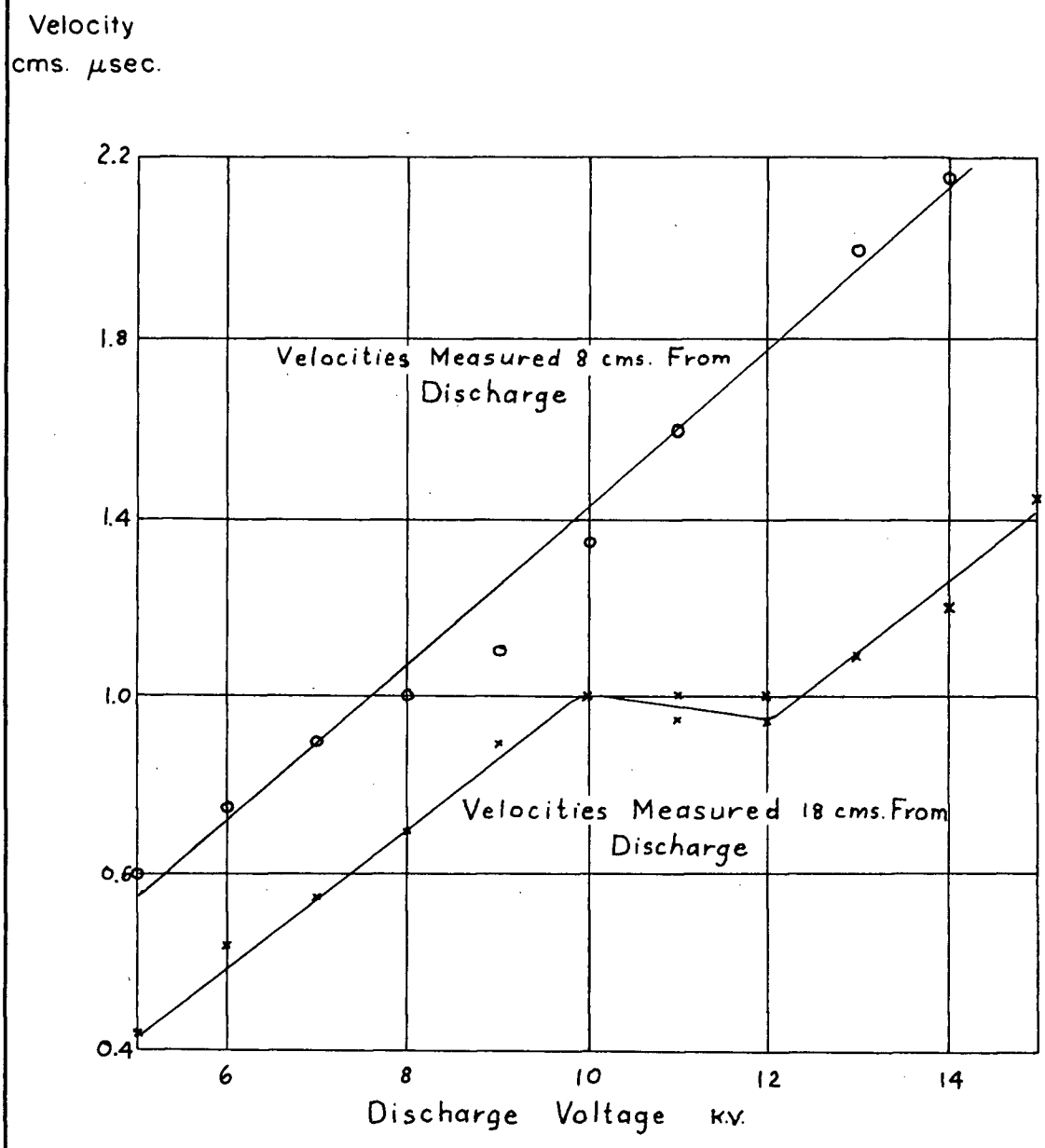

Figure 20: Velocity of Luminosity Front as a Function of Discharge Voltage

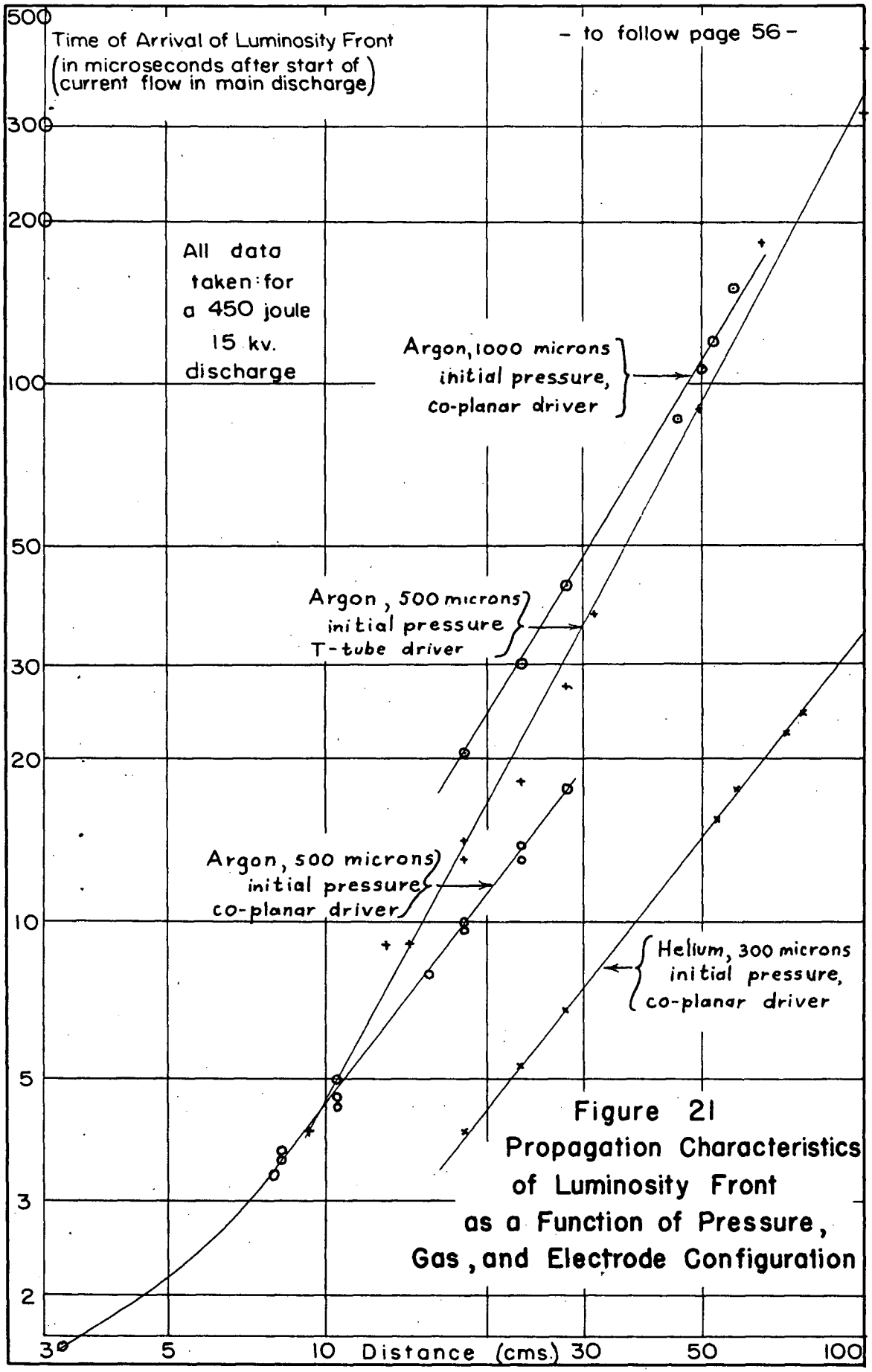

Figure 21
Propagation Characteristics of Luminosity Front as a Function of Pressure, Gas, and Electrode Configuration

estimate of the form of the function g(t) in equation 56. A first approximation can be made by assuming that g(t) is a constant over the first half cycle of the power. Then,

$$E_{\substack{\text{initial}\\ \text{shock}\\ \text{front}}} = \int_0^{\frac{\pi}{2\omega}} \frac{V_o^2 R_\ell C_{Total}}{L_{Total}} \sin^2 \omega t \, dt$$

and assuming $\delta \approx 0$

$$= \frac{\pi}{4} C_{Total} V_o^2 \frac{R_\ell}{\sqrt{\frac{L_{Total}}{C_{Total}}}} \tag{114}$$

If we assume that the shock front energy can be expressed as kinetic energy, then,

$$E_{\substack{\text{initial}\\ \text{shock}\\ \text{front}}} \propto v_s^2 \tag{115}$$

Combining equations 114 and 115 yields,

$$v_s \propto V_o \tag{116}$$

An experimental check of the velocity versus voltage relation resulted in the two curves shown in Figure 20. The velocities were determined by taking the slope of the distance-time luminosity curves at distances of 8 cms and 18 cms from the main discharge. Typical distance-time curves are given in Figure 21. The 8 cm. data lie very close to a straight line so it is strongly suggested that the shock energy is proportional to the square of the initial voltage on the condensers. The discontinuity in the 18 cm. curve can be attributed to decay of the main shock front and then reinforcement by shocks generated by subsequent current pulses. This conclusion was reached from interpretation of the multiple peaks observed with the luminosity detector.

Observation of the decay of the shock waves that follow the initial shock wave has disclosed the interesting property that in helium the subsequent shocks tend to catch up with the initial shock, whereas in argon the subsequent shocks tend to separate both from each other and from the initial shock.

The period of the main discharge is 4.5 microseconds and the peak current 65,000 amperes. The 4 microfarad condenser bank discharges 450 joules. This energy was deposited in the gas sufficiently quickly to result in a shock wave velocity at 10 cms. from the discharge of 5 cms. per microsecond in helium at 300 microns pressure or 2 cms. per microsecond in argon at 500 microns pressure.

The voltage across the base of the coaxial driver built from 1/64 inch copper and measured by the method described in Chapter III, Section 10, revealed that the voltage was almost exactly 90 degrees out of phase with respect to the current after the first quarter of a current cycle - a result that indicated that the impedance of the driver is mostly inductive after the first quarter of a current cycle. From the known value of peak current and the voltage observed across the driver at peak current (that is, at the end of the first quarter cycle) the resistance of the driver could be calculated and was .05 ohms. The inductance could be determined from the ratio of $V/\frac{di}{dt}$ later when the voltage and current are 90 degrees out of phase. The calculated value was 110 millimicrohenries. This value is supposedly the inductance of the driver. However, considering that the total circuit inductance as calculated for the ringing frequency, is only 125 millimicrohenries, it is extremely unlikely that there is only 15 millimicrohenries of inductance in the remainder of the circuit

(condensers, switch and conductors). The more likely explanation is that the observed voltage waveform contains considerable electric field signal because the resistor chain used to observe the voltage was not shielded.

2. The Shock Wave

It has been presupposed throughout all of the experimental work that the shock front velocity (v_s) is approximately equal to the velocity of the luminosity front. Petschek and Byron (1957) present data and theory which confirm that this approximation is valid when v_s is greater than 0.45 cms./microsecond for a shock wave travelling in argon. No similar data has been found by the author for helium. It is thus apparent that it would be very desirable to measure the velocity of the shock front.

The shock front is characterized by an abrupt change in pressure, temperature and density occuring over a distance of a few mean free paths of the gas atoms. The two major methods that have been used by other experimenters to observe the position of the shock front for temperature and density conditions similar to those in the present apparatus are described in detail by Petschek and Byron (1957). Both methods require the introduction of apparatus into the shock tube. It would be a great advantage to be able to detect the shock front with external apparatus so considerable effort has been directed in this direction. Lin, Resler and Kantrowitz (1955) have noted that a pulse of extremely high conductivity (causing a closely spaced plus then minus voltage signal) precedes the main signal caused by ionization of the gas. None of the firings with the present equipment have shown this initial pulse of conductivity. This result favours

the alternative explanation proposed by Lin, Resler and Kantrowitz for their initial signal as being due to electric field pickup. In the present work the 6 turn pickup coil very strongly rejects such signals.

Another method that has been used to detect the shock front at low velocities is to observe the luminosity emitted by the front. Petschek, Rose et al (1955) and Lin, Resler and Kantrowitz observed this low-level luminosity for shock velocities of the order of Mach 8. It has also been observed in the present investigation at velocities of this order with the luminosity detector. The intensity appears to increase with the ambient pressure in front of the shock wave. This luminosity, however, disappears at higher velocities. It would be extremely interesting to obtain a time-resolved spectrum of this radiation - the spectrophotometer is the only piece of equipment that has sufficient sensitivity for such a study. Petschek (1957) suggests but has not conclusively proven that impurities, notably carbon, are responsible for emission of this radiation.

A novel method for detecting the shock front has been proposed and tested by the author. It consists of weakly-ionizing the gas in the shock tube inside the pickup coil used for the conductivity measurements and detecting the signal that results from the motion imparted to the ions by the shock front. No shock front signal has been detected by this method because of limitations in the equipment. The source of the ionizing energy (a 2,450 MC. magnetron-powered radiotherapy unit, model CMD-10 supplied by Raytheon Mfg. Co.) emits a very strong 400 KC signal which conflicts with the desired signal. It is possible that a 400 KC filter could be added to the radiotherapy unit, but this has not been attempted. One result

- to follow page 60 -

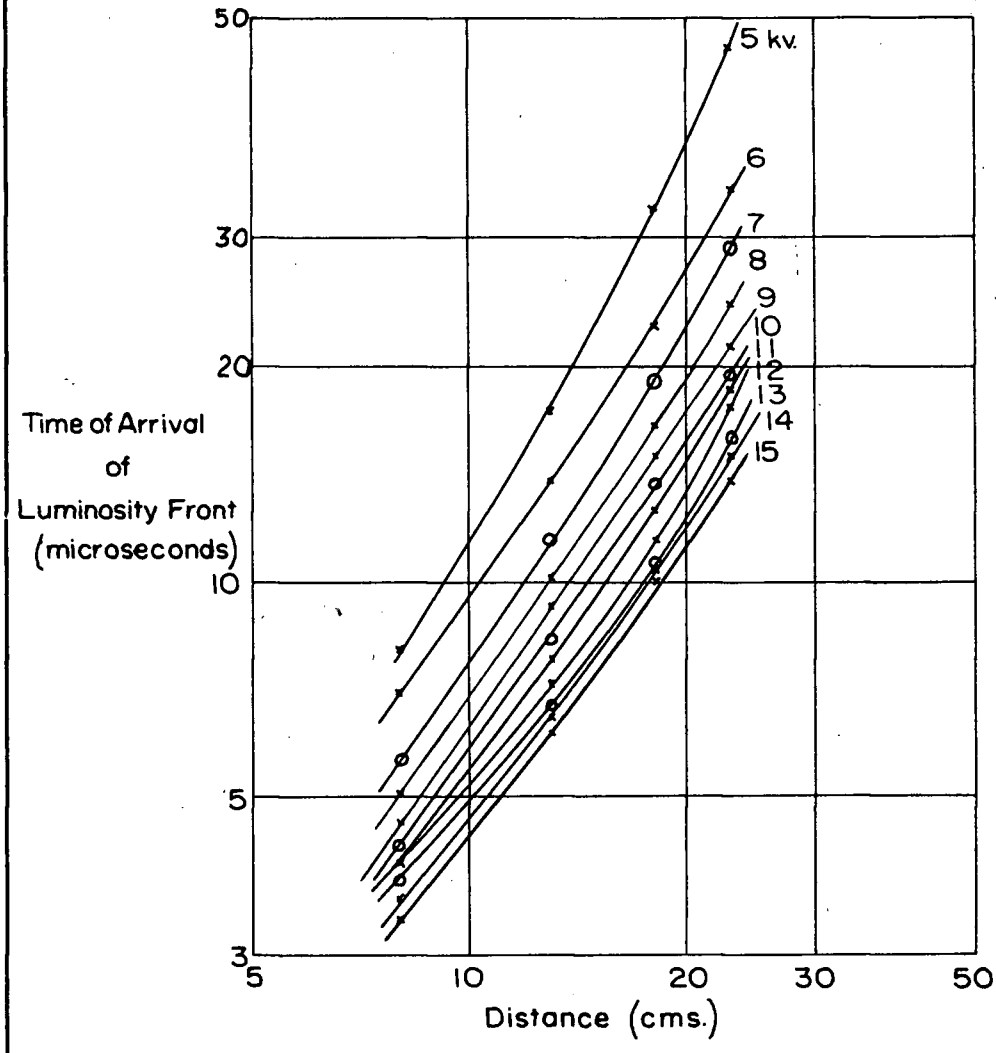

Argon, 500 microns initial pressure, co-planar driver

Figure 22 : Propagation Characteristics of Luminosity Front as a Function of Discharge Voltage

that has come out of these pre-ionization studies is that the rate of ionization of the argon behind the shock front is increased when the gas is pre-ionized.

The shock front can also be detected by interferometry techniques. For a typical case of $\rho_1/\rho_0 = 4$ in an argon shock and over a path length of 2.5 cms. at a wavelength of 5,000°A, the fringe shift is about .02.

Calculations have been made to ascertain the worth of a light refraction system to detect the shock front using a photomultiplier detector. However, the displacement for typical geometry is of the order of .001 mm - far too little to detect even with a photomultiplier and excellent optics.

Graphs showing the propagation characteristics for the luminosity front for various driving conditions are given in Figures 21 and 22.

It is to be noted that the curves all approximately obey the relation

$$x = at^b \tag{117}$$

where a and b are functions of the choice of gas, the ambient pressure and the driving energy. The 15 KV data with the exception of that for the T-Tube system, was taken with the coplanar driving electrodes built from electrode material 1/16 inch thick. The data taken at voltages other than 15 KV was taken from a shock wave driven by a coplanar driver built with 1/64 inch thick electrodes. It is believed that the minor discontinuities in the lines are due to replacement of the leading shock front by subsequent shocks generated by the oscillatory main discharge driver (See Section 1 of the present chapter).

No successful attempt has been made to substantiate equation 117 by a theoretical treatment.

It is believed that the discontinuity in the curves of Figure 21 at a distance of about 10 cms. from the driver is due to the detachment of the shock wave from further driving energy.

The major use of these curves has been to yield the velocity of the luminosity front for any desired condition of operation of the shock tube and at any desired distance from the driver.

Typical waveforms as observed with the luminosity detector are shown in Figure 19.

The electric probes and the conductivity measuring equipment yielded data that was correlated in time with the luminosity data. Thus there was a correspondence between the luminosity and the electron density in the high temperature gas. The electric probe data was analyzed for conductivity for one case. The result was 0.06 mho/cm. for a luminosity front velocity of 0.27 cms./microsecond and an ambient pressure of 500 microns in argon. The temperature immediately behind the shock front that corresponds to this velocity is from equation 11: 6,500°K, and the degree of ionization from equation 17: 10^{-4}. The expected conductivity as calculated by Lin, Resler and Kantrowitz (1955) for this temperature is about 7 mhos/cms. Thus the measured conductivity with the electric probes was greatly in error with respect to the expected conductivity. Lin, Resler and Kantrowitz (1955) obtained similar values and attributed the low values obtained to a low temperature for the gas which is in contact with the probe.

Time-integrated spectra that have been taken have shown that neutral argon atom excitation lines appear at low velocities and that de-excitation lines from singly-ionized argon atoms appear at higher velocities. No lines have been thus far observed that could be attributed to de-excitation from multiple-ionization levels. It is believed that the observed absence of these transitions is due to an extremely rapid thermalization process that very quickly equalizes the atom, electron and ion temperatures once ionization has begun. This equalization process would greatly decrease the atom temperature, typical values being: $T_{max} = 87{,}000^{o}K$, $T_{equ} = 17{,}400^{o}K$. at $\alpha = 0.5$ (from Knorr, 1958, α versus T relation). The temperature of the ions would thus not be high enough for a sufficient time to result in emission of an observable intensity of transitions from multiply-ionized levels.

Although the majority of the experimental work has been on argon, there has been some work done with helium. The velocity of the shock wave is higher in helium than in argon.

The time-integrated spectra have all contained many impurity lines, notably H_α, H_β, H_γ, H_δ, Na I at $5889.95^{o}A$ and $5895.92^{o}A$, Si I at $4128.11^{o}A$ and $4130.96^{o}A$ and C II at $4266.53^{o}A$. The spectra obtained with helium in the shock tube are quite similar to the spectra obtained when argon is the working gas. The major difference is that F II lines are observed from the shock wave in helium gas. The fluorine could be either an impurity supplied in the helium or it could be due to ablation of the teflon in the driving mechanism. Most of the impurity lines have been noticeably broadened. In particular, analysis of the H_α and H_β line profiles should result in extremely useful values for the presently unknown

maximum electron density. The analysis by Griem, Kolb and Shen (1959) can be used to interpret the line profiles.

3. Conductivity

The maximum conductivity, conductivity decay constant and electron temperature during maximum conductivity have been determined for various shock conditions. Typical results are given in Table II and have been determined with the aid of equations 31, 32 and 99 and considering $\alpha = 10^{-4}$ (See Chapter IV, Section 1). It has been found that all terms that contain α in equations 31 and 32 are negligible when $\alpha = 10^{-4}$. We can conclude that maximum conductivity occurs under temperature, pressure, flow velocity and density conditions that are virtually identical to the conditions that exist immediately behind the shock front. Equations 11 and 12 are, therefore, applicable to the conductivity measurements because they are identical to equations 31 and 32 when $\alpha = 10^{-4}$.

Gas	Ionization Front Velocity $= U \approx v_s$ cms. per second	Maximum Axial Magnetic Field Intensity gauss	Maximum Atom Temp. °K.	ψ	β cms.	Maximum Electrical Conductivity mhos/cm.	Calculated Maximum Electron Temp. °K.
Argon 500±20 microns	1.15×10^6	166	119,000	$\frac{1}{.92}$	16	135	60,000
Argon 500±20 microns	1.3×10^6	537	152,000	$\frac{1}{.92}$	16	113	53,000
Helium 280±10 microns	3.3×10^6	344	98,000	$\frac{1}{.92}$	16	180	76,000
Helium 600±50 microns	2.9×10^6	556	76,000	$\frac{1}{.92}$	16	115	53,000

TABLE II: MEASURED VALUES OF MAXIMUM ELECTRICAL CONDUCTIVITY OF PLASMA

The value of the electron temperature in row one of Table II is too high, due to the use of an insufficiently large magnetic field. The magnitude of the magnetic field will determine the choice between equation 99 or 102 as the applicable conductivity-temperature relation. All of the electron temperatures in Table II are probably also in error due to confinement of the plasma by the magnetic field. Confirmation that confinement probably does exist is given by the following conductivity measurements made on argon at an initial pressure of 500 microns and a shock speed of 1.3×10^6 cms./second:

Field Coil Current amperes	V_p volts	$\sigma^* = \left[\frac{I_c v_c^2}{V_{cp}}\right] \frac{V_p}{U \mu_1 I} \psi_1$ in mhos/cm.	B_{max} axial in gauss
0.352	.53	169	35.5
0.960	1.354	152	120
4.30	4.20	113	538

TABLE III: CONDUCTIVITY VERSUS MAGNETIC FIELD INTENSITY

Because the maximum conductivity σ^* is a function of the magnetic field intensity, we can conclude that there is either or both of a confinement effect and that the conductivity of the plasma is a function of the magnetic field. High speed photography of the luminosity associated with the plasma as it passes through the magnetic field would resolve which is the major effect.

Another source of error in the determination of σ^* has been the neglect of both wall cooling and the decrease in velocity due to the wall. Investigation of these errors could be made by studying the conductivity of the plasma when it is propagated down various diameters of shock tube. Again, high speed photographic equipment would be of great help in such an investigation.

A check of any decrease in velocity of the luminosity front caused by the conductivity measurement apparatus has revealed that there is no detectable change in velocity. We can conclude that the magnetic field of the field coils neither appreciably deflects nor changes the energy of the plasma following the shock front.

4. Conclusions

A high velocity shock tube has been assembled and operated. Careful design of the electromagnetic shock driving mechanism has resulted in the attainment of high shock speeds from a comparatively slow and small condenser bank.

The methods that have been employed to measure the properties of the shock wave have proven to be reliable insofar as the results agree with the simple theory that has been presented. Most of the methods have been of a quite general nature and are, therefore, applicable to the study of plasmas generated by other means.

It is suggested that further experimental work be concentrated on obtaining a single shock wave instead of the multiple shock waves generated by the present driver. One promising method consists of shorting the driver with an ignitron at the end of the first current pulse. A second possibility that warrants investigation is the use of a conical driver. Kash et al (1958) have obtained single shock waves with this type of driver.

It would be of great aid in the interpretation of the experimental results if a theoretical solution for two problems could be obtained. Applicable relations are needed for the conductivity, electron density, ion densities, electron temperature, ion temperatures, atom temperature and flow velocity as a function of the distance behind the shock front for different shock velocities. The second problem is to explain the observed shock wave propagation equation in the present tube,

$$x = at^b$$

BIBLIOGRAPHY

Bishop, A.S. (1958) Project Sherwood.

Bostick, W.H. (1958) Boston Conference on Extremely High Temperatures. J. Wiley and Sons, Inc.

Cowling, T.M. (1957) Magnetohydrodynamics.

Din, F. (1956) Thermodynamic Functions of Gases.

Fowler, R.G. et al (1952) Physical Review 88, 137, 1952.

Francis, G. (1956) Handbuch der Physik, Volume 22, 1956.

Gray, D.E. (1957) American Institute of Physics Handbook, 1957.

Griem, H.R., Kolb, A.C. and Shen, K.Y. (1959) Physical Review 116, No.1, 4-16, 1959.

Guman, W.J. (1958) Journal of Applied Physics 29, 109, 1958.

Harris, E.G., et al (1957) Physical Review 105, No. 1, 46-50, 1957.

Hodgman, C.D. (1953-1954) Handbook of Chemistry and Physics.

Inuishi, Y., et al (1957) Journal of Applied Physics 28, 9, 1017, Sept. 1957.

Janes, G.S. and Patrick, R.M. (1958) Boston Conference on Extremely High Temperatures, J. Wiley and Sons, Inc.

Kash, S.W. et al (1958) Velocity Measurements in Magnetically Driven Shock Tubes, a Chapter in the book "The Plasma In a Magnetic Field" by R.K.M. Landshoff.

Klein, M.M. and Bruechner, K.A. (1960) Journal of Applied Physics 31, 1437.

Knorr, G. (1958) Zeitschrift Fur Naturforschung 13a, 941-950, 1958.

Kolb, A.C. (1957) Physical Review 107, 345, 1957.

Kolb, A.C. (August 1957) Physical Review 107, 1197, 1957.

Kolb, A.C. per Landshoff, R.K.M. (1957) Experiments at U.S. Naval Research Laboratory, a Chapter in the book "Magnetohydrodynamics" by R.K.M. Landshoff.

Kolb, A.C. (1958) Geneva Conference Paper (1958) P/345. Reprinted in Progress in Nuclear Energy Series XI, 1959.

Levine, M.A., Sampson, J.L., Waniek, R.W. (1958) Boston Conference on Extremely High Temperatures, J. Wiley and Sons, Inc.

Lin, S-C., Resler, E.L., and Kantrowitz, A. (1955) Journal of Applied Physics 26,95, 1955.

Loeb, L.B. (1955) Basic Processes of Gaseous Electronics, 1955.

Morse, P.M. (1948) Vibration and Sound.

Olsen, H.N. and Huxford, W.S. (1952) Physical Review 87, 922, 1952.

Penner, S.S., Harshbarger, F., and Vali, V. (1957) Combustion Researches and Reviews, 1957.

Perry, J.H. (1941) Chemical Engineer's Handbook.

Petschek, H.E., Rose, P.H., et al (1955) Journal of Applied Physics 26, 83, 1955.

Petschek, H.E. and Byron, S. (1957) Annals of Physics 1, 270-315, 1957.

Resler, E.L., Lin, S-C., and Kantrowitz, A. (1952) Journal of Applied Physics 23, 1390, 1952.

Scott, F.R. and Wenzel, R.F. (1960) Physical Review 119, No. 4, 1187-1188, 1960.

Smith, V.L. (1960) I.R.E. Transactions Nuclear Science NS-7, 13, 1960.

Spitzer, L. (1956) Physics of Fully Ionized Gases.